



Article submitted to journal

**Subject Areas:**physics, condensed matter,  
superconductivity**Keywords:**surface bound states, film geometry,  
non-uniform superfluid**Author for correspondence:**

Anton Vorontsov

e-mail:

avorontsov@physics.montana.edu

Andreev Bound States in  
Superconducting Films and  
Confined Superfluid  $^3\text{He}$ Anton B. Vorontsov<sup>1</sup><sup>1</sup>Department of Physics, Montana State University,  
Bozeman, Montana 59717, USA

This paper reviews the confinement-driven phase transitions, and the prediction of superfluid phases with broken time-reversal or translational symmetry in thin films. The new phases are a result of particle-hole coherent Andreev scattering processes that create quasiparticle states with energies inside the superconducting gap. These states cause profound restructuring of the low-energy spectrum in the surface region of several coherence lengths  $\xi_0$  with large spatial variations of the superconducting order parameter. In confined geometry, such as slabs, films, pores, or nano-dots, with one or more physical dimensions  $D \sim 10\xi_0$ , Andreev bound states can dominate properties of the superfluid phases, leading to modified experimental signatures. They can dramatically change the energy landscape, and drive transitions into new superfluid phases, that are typically unstable in the bulk superfluid. On the examples of single-component singlet  $d$ -wave superconductor, and triplet multi-component superfluid  $^3\text{He}$  I show how properties of condensed phases in restricted geometry depend on the order parameter structure. I will highlight the connection between Andreev bound states and confinement-stabilized phases with additional broken symmetries, describe recent progress and open questions in theoretical and experimental investigation of superfluids in confined geometry.

## 1. Introduction

Majority of known superconductors, including ones with the highest and lowest measured transition temperatures, as well as superfluid  $^3\text{He}$ , belong to the class of unconventional pairing states. [1] By definition, they break multiple symmetries of the high-temperature normal phase, that usually include the  $U(1)$  symmetry, rotations and reflections determined by the crystal symmetry group, and rotations in spin space. These superconductors develop order parameter (OP) that beside having a definite phase resulting from broken global  $U(1)$  symmetry, possess non-trivial structure in momentum and spin spaces. These broken symmetries manifest themselves in characteristic low-energy spectrum of quasiparticles, and show up in thermodynamic, magnetic, transport properties of unconventional materials.

The low-energy excitations above the ground state of a condensate of Cooper pairs, are combinations of particles and holes, that can be written as a sum of creation and annihilation operators,  $\alpha_{\mathbf{p}s}^\dagger |G.S.\rangle = \left( u_{\mathbf{p}ss'}^* a_{\mathbf{p}s'}^\dagger - v_{\mathbf{p}ss'}^* a_{-\mathbf{p}s'} \right) |G.S.\rangle = E_{\mathbf{p}} |G.S.\rangle$ , with excitation energies  $E_{\mathbf{p}} = \sqrt{v_f^2(p - p_f)^2 + |\Delta(\mathbf{p}_f)|^2}$  indirectly reflecting broken symmetries of the order parameter  $\Delta(\mathbf{p}_f)$  and type of the pairing interactions.

Scattering of these quasiparticles on the boundaries, surfaces or interfaces, lead to further modification of the condensate properties. Spatial variations of the superconducting order parameter  $\Delta(\mathbf{R}, \mathbf{p}_f)$ , caused by the boundary conditions or other competing effects, result in a new kind of scattering processes. The quasiparticles can convert between particles and holes, transferring weight between (spin-matrix) amplitudes  $u_{\mathbf{p}ss'} \leftrightarrow v_{\mathbf{p}ss'}$  [2]. These scattering processes originate in the particle-hole coherence of superconductors, and they play important role in non-uniform superconducting environments. These are the most important scattering events for the low-energy sector, resulting in new quasiparticle states below the bulk gap edge and bound to the inhomogeneous regions, whose properties will dominate the physics of the boundary region. [3–5] The new quasiparticle spectrum leads to strong order parameter variations on the coherence length scale  $\xi_0 = \hbar v_f / 2\pi k_B T_c$ .

The new quasiparticle states that arise in the boundary regions can be broadly divided into two categories. One type of states is determined by the properties of the superconductors in the bulk, and largely independent of the order parameter suppression near the surface. In that sense they are determined by the far away regions, as in a domain wall and thus have a more of a topological character, similar to mass term change in relativistic Dirac equation [6], These states can have any energy-momentum dispersion, depending on the orientation of the surface, and initial and final values of the order parameter along incoming and outgoing quasiparticle's trajectories. The second class is the one that was considered by Andreev originally, where quasiparticles experience multiple reflections inside the effective potential well created by the suppression of the OP amplitude. This typically leads to bound states with energies not too far below the gap edge.

Quasiparticle states with subgap energies, bound to the surface region of several coherence lengths, have a profound effect on physical properties. Examples include presence of a subdominant channel  $d + is$  near surface that leads to splitting of the zero-energy states and generation of current-carrying state that breaks time-reversal symmetry. [7,8] Surface ABS carry paramagnetic currents that run in the opposite direction to the usual superconducting screening currents, which shows up in the anomalous behavior of the penetration depth. [8,9] Interaction of bound states with self-induced magnetic field leads to lowering of energy in the surface region and spontaneous generation of currents on penetration length scale. [10–13] In quantum wires, Andreev bound states (ABS) can lead to new pairing states with spin-triplet character. [14]

Even more profound are effects of the bound states on the properties of superconductors and superfluids in confined geometry, such as films, slabs, pores and nano-dots. If geometrical dimensions of a sample are several coherence lengths, the order parameter suppression is significant in the entire volume, and the spectrum of low-energy excitations is very different from

that of bulk superfluid, is mostly dominated by the quasiparticle states that scatter off the surfaces. This results in a significant modifications of the thermodynamic and non-equilibrium properties, and shows up in NMR, heat capacity, collective mode dynamics, and other experimental probes.

Moreover, due to significantly modified order parameter and quasiparticle spectrum, the landscape of free energy is changed as well. Additional constraints imposed by the boundary conditions make bulk phases considerably less favorable, and make room for new phases that have the lowest energy state in the new landscape. One of the most interesting possibilities is appearance of states that have symmetry or topological properties different from those of the bulk phases.

The many effects associated with the bound states, and their sensitivity to the nature of the pairing, surface geometry, makes investigation of properties of superfluids in confinement both challenging and interesting. Spatially constrained superfluids and geometry manipulation provide new ways to learn about properties of unconventional superconductors, insight into the nature of superconducting pairing, and possibility of generating new superfluid phases. Manipulation of the surface states can change electronic transport across superconductor-normal interfaces and promise better control of small-scale superconducting systems, opening possibilities to utilize them in new devices.

In this review I describe properties of unconventional superconductors in thin films, and highlight the connection between unusual properties of the confined superfluids with the presence and structure of Andreev bound states spectrum. In section 2 a brief summary of theoretical approach to study non-uniform superconductors is given. In section 3 I discuss the structure of new phases that are expected to appear in thin films of unconventional superconductors and superfluid  $^3\text{He}$ . Finally, in part 4, I outline recent development in experimental techniques that are oriented to better understanding and control of quasiparticle states and superfluid phases in confinement.

## 2. Surface bound states near surfaces and in domain walls

Investigation of superfluid condensates in confined geometry requires careful treatment of multiple aspects of the physics, that influence the energy balance. To calculate details of the order parameter suppression precisely, one needs to specify scattering properties of the surfaces, their shape and orientation, and size of the container. Other parameters, such as dimensionality of the geometry, shape of the Fermi surface, external fields or other pairbreaking effects, and strong-coupling corrections, all can affect the energetics and may favor different phases.

Early theoretical investigation of pairing states in constrained geometry focused on properties of superfluid  $^3\text{He}$ . Boundary conditions for the order parameter in the A-phase were proposed in [15], and suppression of the transition temperature calculated [16], based on de Gennes' formulation of inhomogeneous superfluidity in terms of semiclassical correlation functions. Later investigation of superfluid phases in slabs and cylindrical pores used Ginzburg-Landau (GL) approach [17–20]. Properties of the superflow and NMR responses of confined  $^3\text{He}$  were calculated [21]. Although the GL equations have a limited applicability range, they have an advantage of being the simplest approach to inhomogeneous problems in the long-wavelength limit, and can easily include the strong-coupling corrections via phenomenological parameters.

A more sophisticated technique to address strongly non-uniform states is based on the quasiclassical Green's functions. [22–24] The quasiclassical theory has been used to study confined superfluids extensively, since it is applicable to various phenomena under a broad range of conditions, including arbitrary temperatures, fields, and systems out of equilibrium.  $^3\text{He}$  flow and superfluid density in film geometry have been investigated in [25–28]; the A-B transition in thin films was discussed in [29–31]; a detailed analysis of thermodynamic properties of the A-phase was presented in [31]; study of thermodynamic properties and Majorana signatures of distorted  $^3\text{He}$ -A and  $^3\text{He}$ -B phases in narrow channels and slabs was done in [32,33].

For completeness we briefly summarize the main points of the technique: the quasiclassical propagator (Green's function)  $\hat{g}(\mathbf{R}, \mathbf{p}_f; \epsilon)$  describes quasiparticle correlations on the scale  $\hbar/p_f \ll |\delta \mathbf{R}| \sim \xi_0 = \hbar v_f / 2\pi k_B T_c$ , with energy  $\epsilon$ , along a quasiparticle's classical trajectory defined by velocity  $\mathbf{v}_f$  on the Fermi surface at point  $\mathbf{p}_f$ . It satisfies Eilenberger transport equation and normalization condition:

$$[\epsilon \hat{\tau}_3 - \hat{\Delta}, \hat{g}] + i\hbar \mathbf{v}_f \cdot \nabla_{\mathbf{R}} \hat{g} = 0, \quad \hat{g}^2 = -\pi^2. \quad (2.1)$$

The propagator has  $4 \times 4$  matrix structure in particle-hole and spin space, denoted here by wide hat. We only consider mean-field self-energies that describe the superconducting order parameter,

$$\hat{g} = \begin{pmatrix} \hat{g} & \hat{f} \\ \hat{f} & \hat{g} \end{pmatrix}, \quad \hat{\Delta} = \begin{pmatrix} 0 & \hat{\Delta}_{\mathbf{p}} \\ \hat{\Delta}_{\mathbf{p}} & 0 \end{pmatrix}, \quad (2.2)$$

where the  $2 \times 2$  spin structure of the order parameter, denoted by narrow hat, for singlet state is  $\hat{\Delta} = \Delta_{\mathbf{p}}(i\sigma_y)$  and for triplet is  $\hat{\Delta} = \Delta_{\mathbf{p}}(i\sigma\sigma_y)$ . The energy can be shifted up or down in the complex plane to obtain Retarded ( $\epsilon + i0$ ), Advanced ( $\epsilon - i0$ ), or finite temperature Matsubara Green's functions ( $\epsilon \rightarrow i\epsilon_m = i\pi T(2m + 1)$ ). The particle-hole components of the propagator are related through symmetry [24] that we denote by underline-operation, which we write for complex energy that combines both Retarded/Advanced and Matsubara representations:

$$\underline{\hat{g}}(\mathbf{R}, \mathbf{p}_f; \epsilon + i\epsilon_m) = \hat{g}(\mathbf{R}, -\mathbf{p}_f; -\epsilon + i\epsilon_m)^*. \quad (2.3)$$

This symmetry relates objects in the same half-plane of the complex energy. In addition, there is another symmetry that relates propagator components in the upper and lower half-planes:

$$\hat{g}(\mathbf{R}, \mathbf{p}_f; \epsilon + i\epsilon_m)^\dagger = \hat{g}(\mathbf{R}, \mathbf{p}_f; \epsilon - i\epsilon_m), \quad \hat{f}(\mathbf{R}, \mathbf{p}_f; \epsilon + i\epsilon_m)^\dagger = -\underline{\hat{f}}(\mathbf{R}, \mathbf{p}_f; \epsilon - i\epsilon_m). \quad (2.4)$$

Calculation of the equilibrium order parameter is most conveniently done using Matsubara technique. Equation (2.1) for  $\hat{g}$  has to be solved self-consistently with the equation for the order parameter. If the pairing interaction is separable with basis functions in momentum space  $\mathcal{V}(\mathbf{p}_f)$ , this equation for singlet pairing has the form:

$$\Delta(\mathbf{R}, \mathbf{p}_f) = T \sum_{|\epsilon_m| < \Lambda} N_f \langle V \mathcal{V}(\mathbf{p}_f) \mathcal{V}^*(\mathbf{p}'_f) f(\mathbf{R}, \mathbf{p}'_f; i\epsilon_m) \rangle_{\mathbf{p}'_f} \quad (2.5)$$

with attractive pairing interaction  $V > 0$ , cut off at energy  $\Lambda$ . Angle brackets traditionally denote Fermi surface integration, and  $N_f$  is density of states at the Fermi level per one spin projection.

The most convenient numerical route to solve the transport equations (2.1) is to use parametrization of the Green's function in terms of the coherence amplitudes, that are chosen to automatically satisfy the normalization condition. Following notation in [34]:

$$\hat{g}(\mathbf{R}, \mathbf{p}_f; \epsilon) = \mp i\pi \begin{pmatrix} (1 - \hat{\gamma}\hat{\gamma})^{-1} & 0 \\ 0 & (1 - \hat{\gamma}\hat{\gamma})^{-1} \end{pmatrix} \begin{pmatrix} (1 + \hat{\gamma}\hat{\gamma}) & 2\hat{\gamma} \\ -2\hat{\gamma} & -(1 + \hat{\gamma}\hat{\gamma}) \end{pmatrix}, \quad (2.6)$$

where  $\epsilon = \epsilon' + i\epsilon''$  is fully complex, and  $(-1)$  sign applies to upper half plane  $\epsilon'' > 0$ , while  $(+1)$  sign is used for  $\epsilon'' < 0$  functions. The coherence amplitudes are  $2 \times 2$  matrices in spin space, satisfying symmetries that follow from (2.3) and (2.4)

$$\begin{aligned} \underline{\hat{\gamma}}(\mathbf{R}, \mathbf{p}_f; \epsilon' + i\epsilon'') &= \hat{\gamma}(\mathbf{R}, -\mathbf{p}_f; -\epsilon' + i\epsilon'')^*, \\ \hat{\gamma}(\mathbf{R}, \mathbf{p}_f; \epsilon' + i\epsilon'') &= \hat{\gamma}(\mathbf{R}, \mathbf{p}_f; \epsilon' - i\epsilon'')^\dagger, \end{aligned} \quad (2.7)$$

and obeying non-linear differential equation of Riccati type,

$$\begin{aligned} i\hbar \mathbf{v}_f \cdot \nabla \hat{\gamma} + 2\epsilon \hat{\gamma} &= \hat{\gamma} \hat{\Delta} \hat{\gamma} - \hat{\Delta}, \\ i\hbar \mathbf{v}_f \cdot \nabla \underline{\hat{\gamma}} - 2\epsilon \underline{\hat{\gamma}} &= \underline{\hat{\gamma}} \hat{\Delta} \underline{\hat{\gamma}} - \underline{\hat{\Delta}}. \end{aligned} \quad (2.8)$$

These functions carry information about particle-hole coherence and can be expressed through Andreev amplitudes, for example  $\hat{\gamma} = \hat{u}^{-1} \hat{v}$  [34]. For retarded functions ( $Im(\epsilon) > 0$ ), the

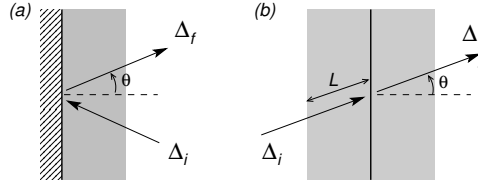


**Figure 1.** The quasiclassical trajectories at a specular surface or completely transparent domain wall. The propagator at the surface/interface is determined by the coherence amplitudes  $\hat{\gamma}_i$  integrated along the incoming trajectory, and  $\hat{\gamma}_f$  integrated opposite the outgoing trajectory (retarded functions). The order parameter configurations along two trajectories far away from the interface determine the ‘topological’ aspect of the bound states; whereas the region of suppressed order parameter of typical lengths  $L \sim 5\xi_0 / \cos \theta$  along a trajectory, determines multiple-reflected quasiparticle states in effective order parameter potential well. The coherence length is defined as  $\xi_0 = \hbar v_f / 2\pi k_B T_c$ .

integration of these equations are done along the straight classical trajectory in direction of Fermi velocity  $\mathbf{v}_f$  for  $\hat{\gamma}$ , and in  $-\mathbf{v}_f$  direction for  $\hat{\bar{\gamma}}$ . In unitary superfluids  $\hat{\Delta}\hat{\bar{\Delta}} = -|\Delta(\mathbf{p}_f)|^2 \hat{1}$ , solution for amplitudes in uniform state are:

$$\hat{\gamma}(\mathbf{p}_f; \epsilon) = -\frac{\hat{\Delta}(\mathbf{p}_f)}{\epsilon \pm i\sqrt{|\Delta(\mathbf{p}_f)|^2 - \epsilon^2}}, \quad \hat{\bar{\gamma}}(\mathbf{p}_f; \epsilon) = \frac{\hat{\bar{\Delta}}(\mathbf{p}_f)}{\epsilon \pm i\sqrt{|\Delta(\mathbf{p}_f)|^2 - \epsilon^2}}, \quad (2.9)$$

with the signs distinguishing between positive/negative  $Im(\epsilon)$ . These solutions are taken as initial values for the coherence amplitudes far away from the interface.

Integration of the transport equations require boundary conditions for the propagators, or for the coherence amplitudes. There exist several models that are based on different physical pictures of the scattering process at a surface. For atomically smooth surface the parallel momentum is conserved and the reflection is mirror-like, or specular. In this case both the propagator and the coherence amplitudes are continuous across the reflection point. For atomically rough surfaces one can use ‘randomly rippled wall’ model [35–37], diffuse boundary with thin layer of atomic-size impurities coating a smooth surface [25,38], ‘randomly oriented mirror’ model [39], and a universal model based on scattering S-matrix approach that can describe partial specular-diffuse reflection [40,41]. Typically, various implementations of boundary conditions give similar results for the order parameter but somewhat different quasiparticle spectra. Most recent formulation of the boundary conditions is due to M. Eschrig, who described an S-matrix approach to scattering in terms of coherence amplitudes [42].

Using Riccati amplitude parametrization of the Green’s functions it is particularly straightforward to estimate the local density of states (DOS) and obtain structure of the bound states spectrum at specular boundary or completely transparent interface, Fig. 1. The spin-matrix density of states is defined as  $\hat{N}(\mathbf{R}, \mathbf{p}_f; \epsilon) = -(1/\pi) Im \hat{g}(\mathbf{R}, \mathbf{p}_f; \epsilon)$  and at the surface is determined by:

$$\hat{g}^R(\mathbf{R} = 0, \mathbf{p}_f; \epsilon) = -i\pi \frac{1 + \hat{\gamma}(0, \mathbf{p}_f; \epsilon)\hat{\bar{\gamma}}(0, \mathbf{p}_f; \epsilon)}{1 - \hat{\gamma}(0, \mathbf{p}_f; \epsilon)\hat{\bar{\gamma}}(0, \mathbf{p}_f; \epsilon)} \quad (2.10)$$

Neglecting the suppression of the order parameter near the interface, we can approximate the coherence amplitudes by their uniform values Eq. (2.9) far from the interface in final and initial points of a trajectory:  $\hat{\gamma}(0, \mathbf{p}_f; \epsilon) = \hat{\gamma}_i$  and  $\hat{\bar{\gamma}}(0, \mathbf{p}_f; \epsilon) = \hat{\bar{\gamma}}_f$ , where we assume the coherence amplitude is continuous along the trajectory at  $\mathbf{R} = 0$ , thus the same value of the momentum  $\mathbf{p}_f$ .

In singlet superconductors with one OP component this leads to condition on the poles of the Green’s function  $\hat{g}(0)$  at the surface

$$1 - \hat{\gamma}_i \hat{\bar{\gamma}}_f = 1 - \frac{\Delta_i \Delta_f^*}{[\epsilon + i\sqrt{|\Delta_i|^2 - \epsilon^2}][\epsilon + i\sqrt{|\Delta_f|^2 - \epsilon^2}]} = 0. \quad (2.11)$$

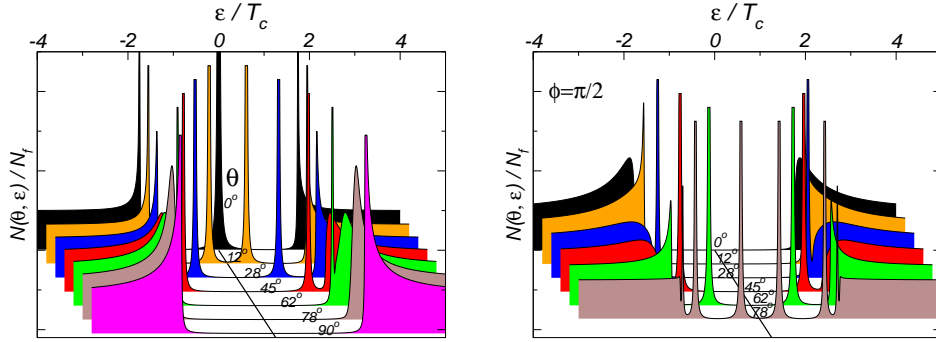


**Figure 2.** The angle-resolved DOS in domain walls between degenerate states of superfluid  $^3\text{He-B}$ . On the left, quasiparticles that travel across domain wall (transverse direction), experience OP sign change. This configuration also gives spectrum at a specular surface. The bound states form a cone in momentum-energy space Eq. (2.16). In the right panel, one of the parallel OP components ( $y$  in this case) changes sign, resulting in bound states near continuum edge, shown here for  $\hat{p}_x = 0$ , Eq. (2.17).

The spectrum of bound states for parametrization  $\Delta_i = \Delta e^{+i\varphi/2}$ ,  $\Delta_f = \Delta e^{-i\varphi/2}$  is:

$$1 - \left[ \frac{\Delta e^{+i\varphi/2}}{\epsilon + i\sqrt{\Delta^2 - \epsilon^2}} \right]^2 = 0 \quad \Rightarrow \quad \epsilon = \pm \Delta \cos \frac{\varphi}{2} \quad (2.12)$$

which gives well-known zero-energy states for trajectories that connect order parameter values with relative phase  $\pi$  [43].

As another example, we consider interface between two degenerate states of  $^3\text{He-B}$ . The two states have the same energy gap, but generally have order parameter that has an invariant part  $\Delta_+$  and a sign-changing part  $\Delta_-$  on two sides:  $\Delta_i = \Delta_+ - \Delta_-$ ,  $\Delta_f = \Delta_+ + \Delta_-$ , with  $\Delta_i^2 = \Delta_f^2 = \Delta_+^2 + \Delta_-^2 \equiv \Delta^2$ . The denominator of the diagonal propagator  $\hat{g}(0)$  is

$$1 - \hat{\gamma}_i \hat{\gamma}_f = 1 - \frac{(\Delta_i \sigma)(\Delta_f \sigma)}{[\epsilon + i\sqrt{\Delta^2 - \epsilon^2}]^2} = 1 - \frac{\Delta_i \cdot \Delta_f + i\sigma(\Delta_i \times \Delta_f)}{[\epsilon + i\sqrt{\Delta^2 - \epsilon^2}]^2} = 0. \quad (2.13)$$

The spin structure of the bound states is determined by cross product of spin vectors in final and initial points of the trajectory,  $\propto (\Delta_i \times \Delta_f)$ , and the energies of the bound states follow from poles of  $(1 - \hat{\gamma}_i \hat{\gamma}_f)^{-1}$ :

$$\left[ 1 - \frac{\Delta_+^2 - \Delta_-^2}{(\epsilon + i\sqrt{\Delta^2 - \epsilon^2})^2} \right]^2 + \left[ \frac{2\Delta_+ \times \Delta_-}{(\epsilon + i\sqrt{\Delta^2 - \epsilon^2})^2} \right]^2 = 0. \quad (2.14)$$

After re-arranging this gives bound state energies:

$$2\epsilon^2 - 2\Delta_+^2 + 2i\epsilon\sqrt{\Delta^2 - \epsilon^2} = \pm i2|\Delta_+||\Delta_-| \quad \Rightarrow \quad \epsilon = \pm |\Delta_+|, \quad (2.15)$$

- determined by the order parameter component that remains invariant in the reflection/transmission process. We use it evaluate DOS for two domain wall configurations that are relevant to the film geometry. Plane  $xy$  separates two domains at  $z < 0$  and  $z > 0$ . In the first configuration the ‘normal’ OP component changes sign: from  $\Delta_i(z = -\infty) = (\Delta_0 \hat{p}_x, \Delta_0 \hat{p}_y, -\Delta_0 \hat{p}_z)$  to  $\Delta_f(z = +\infty) = (\Delta_0 \hat{p}_x, \Delta_0 \hat{p}_y, +\Delta_0 \hat{p}_z)$ , resulting in the bound states energies

$$\epsilon_{\perp} = \pm \Delta_0 \sqrt{\hat{p}_x^2 + \hat{p}_y^2} = \pm \Delta_0 \sin \theta. \quad (2.16)$$

In second configuration, quasiparticle that travel ‘parallel’ to the wall experience the sign change, from  $\Delta_i(z = -\infty) = (\Delta_0 \hat{p}_x, -\Delta_0 \hat{p}_y, \Delta_0 \hat{p}_z)$  to  $\Delta_f(z = +\infty) = (\Delta_0 \hat{p}_x, +\Delta_0 \hat{p}_y, \Delta_0 \hat{p}_z)$ , and form bound states with

$$\epsilon_{||} = \pm \Delta_0 \sqrt{\hat{p}_z^2 + \hat{p}_x^2} = \pm \Delta_0 \sqrt{\cos^2 \theta + \sin^2 \theta \cos^2 \phi}. \quad (2.17)$$

The angle resolved DOS for the two domain walls from self-consistent numerical calculation is shown in Fig. 2. The approximate calculation of bound states energies agrees with it quite well. The bound states in ‘parallel’ configuration in general lie closer to the continuum states and result in a lower energy for this domain wall (see also section 3(b)).

The above states arise from the ‘topological’ properties of the particular domain wall or surface orientation. To include other bound states that appear as a result of multiple particle-hole reflections inside the OP suppression region, or to find DOS at arbitrary distance from the surface, one should know the coherence amplitudes everywhere along a trajectory. For a piecewise order parameter profile this can be done using a property of Riccati equations. In a region with  $\hat{\Delta}_0 = \text{const}$  and known uniform solution  $\hat{\gamma}_0$ , solution for  $\hat{\gamma}$  with (another) initial value  $\hat{\gamma}(0)$  has the form  $\hat{\gamma} = \hat{\gamma}_0 + \hat{z}^{-1}$  with auxiliary function  $\hat{z}$  having initial value  $\hat{z}(0) = (\hat{\gamma}(0) - \hat{\gamma}_0)^{-1}$  and satisfying linear equation that is more readily solved than non-linear one:

$$-i\hbar \mathbf{v}_f \nabla \hat{z} + 2\epsilon \hat{z} = \hat{\Delta}_0 \hat{\gamma}_0 \hat{z} + \hat{z} \hat{\gamma}_0 \hat{\Delta}_0 + \hat{\Delta}_0. \quad (2.18)$$

Finally, to determine the relative stability of different phases, one needs to calculate the free energy, given an OP configuration. This can be done using the Eilenberger functional [22], or one of the approaches based on the Luttinger-Ward functional with differentiation with respect to coupling constant, as applied to thin films of  $^3\text{He-A}$  [31], or differentiation with respect to the energy, as described in application to multi-order pnictide materials [44].

### 3. New superfluid phases in confined geometry

Within about  $5 - 10\xi_0$  of a pairbreaking surface, the order parameter is strongly suppressed, and a re-distribution of the quasiparticle spectrum takes place. States from continuum are shifted below the gap and appear as bound states. As the spectrum is modified, significant changes occur to the thermodynamic and transport properties in this region. If a superconducting state is confined to a slab only two to three times larger than  $5 - 10\xi_0$  then the pairbreaking influence of the surfaces extends over the entire volume of the sample and one expects that the changes in properties of superconducting state will be detectable. Some of the changes constitute a somewhat ‘trivial’ modification of the superfluid phases, that does not strongly affect the overall structure and symmetry of the condensate. Despite this, such modifications are interesting in themselves from another perspective: Andreev bound states reflect the non-trivial topological aspects of the underlying superfluid phases, as shown, for example, by investigating angular momentum in discs of chiral superfluid [45,46], or superflow in narrow channels [32,33].

The other, more dramatic effect of strong confinement and large overall suppression of order parameter, is the possibility of appearance of new phases with different symmetry properties compared with the bulk phases. Andreev bound states also play the key role here, as the new order parameter configurations and new broken symmetries are determined by the changes in energies of these states.

Prediction of appearance, and investigation of new phases in confined geometry usually falls outside the scope of the traditionally employed GL theory, that has only lowest gradient terms,  $|\nabla \Delta|^2 \ll |\Delta|^2/\xi_0^2$ . The strong confinement is associated with fast changing order parameter and large influence of the gradient energy terms in the free energy functional. This indicates a great importance of non-local effects for these phenomena. In nodal superconductors non-locality can play especially important role since coherence length along nodal directions is very long, resulting, for example, in a modified temperature behavior of penetration depth. [47]

These non-local effects can be interpreted as interaction of Andreev bound states across the width of the slab, and can result in self-generation of bound states and currents in a semi-infinite



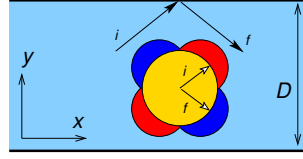


**Figure 3.** A superconducting wire/slab of thickness  $D$  with strongly pairbreaking surfaces.

material. The new superfluid states that appear in constrained environment have lower symmetry than allowed by geometry. Nature of the new broken symmetry depends on the properties of the pairing interaction, its symmetry and number of order parameter components, as well as the background superfluid phases. Below we describe two examples, where the additional broken symmetries are time-reversal symmetry and spatial translation symmetry.

### (a) Singlet superconductors

We first discuss confinement of a one-component singlet  $d$ -wave superconductor between two specular pairbreaking surfaces, Fig. 3, where the order parameter is  $\Delta(\mathbf{R}, \mathbf{p}_f) = \Delta(y)\mathcal{Y}(\mathbf{p}_f)$  and  $\mathcal{Y}(\mathbf{p}_f) = \sin 2\phi_p$  is the basis function ( $\tan \phi_p = \hat{p}_y/\hat{p}_x$ ). This simple system clearly demonstrates effects of confinement on Andreev bound states and the role they play in generating phases with additional broken symmetries.

We start by looking at the confinement-induced transition between superconducting and normal phases. A complete description of the superconducting state requires self-consistent calculation of the non-uniform order parameter. Spatial profiles of the gap function  $\Delta(y)$  for films of various slab thicknesses  $D$ , obtained using quasiclassical theory, are shown on the left in Fig. 4. As the slab becomes narrower, superconductivity gets suppressed and disappears below about  $D \sim 7\xi_0$  (for temperature  $T/T_c = 0.2$ ).

It is convenient to introduce a parameter measuring confinement, or inverse thickness,  $\tilde{Q} \equiv \pi\xi_0/D$ , and plot the N-SC transition in confinement vs temperature plane, shown on the right of Fig. 4. When  $\tilde{Q} = 0$  the system is infinite, or semi-infinite, transition  $T_c$  is that of the bulk system. As confinement increases the transition temperature is suppressed. However, in thin films there is a range of re-entrance of the normal phase,  $0.44 \lesssim \tilde{Q} \lesssim 0.51$ , see also [48]. If one traverses this region toward lower  $T$ , the order parameter first appears and grows, but then starts to drop, smoothly disappearing at re-entrance of the normal state. The free energy is lower than the normal state value along this path, as shown in the insets of the right panel of Fig. 4.

To understand details of this transition, why back-bending feature appears and whether it is physical, one should derive a free energy functional expansion in small order parameter  $\Delta$ , keeping gradient energy terms to all orders, since they play the main role, as we will see. Expanding the order parameter into plane wave basis

$$\Delta(\mathbf{R}, \mathbf{p}_f) = \mathcal{Y}(\mathbf{p}_f) \sum_{\mathbf{q}} \Delta_{\mathbf{q}} e^{i\mathbf{q}\mathbf{R}}$$

we can integrate back the self-consistency equation to obtain the free energy functional:

$$\frac{\delta \Delta F}{\delta \Delta_{\mathbf{q}}^*} \equiv \Delta_{\mathbf{q}} \left\langle \mathcal{Y}(\mathbf{p}_f)^2 \right\rangle \ln \frac{T}{T_c} - T \sum_{\epsilon_m} \left\langle \mathcal{Y}(\mathbf{p}_f) \left( f_{\mathbf{q}}(\mathbf{p}_f; \epsilon_m) - \frac{\pi \Delta_{\mathbf{q}} \mathcal{Y}(\mathbf{p}_f)}{|\epsilon_m|} \right) \right\rangle = 0. \quad (3.1)$$

Here  $\epsilon_m = \pi T(2m+1)$  - Matsubara energy, and brackets denote angle average over circle Fermi surface,  $\langle \dots \rangle = \int \frac{d\phi_p}{2\pi} \dots$ . To get the free energy, we need to solve the quasiclassical equations to third order in  $\Delta_{\mathbf{q}}$ . The diagonal,  $g$ , and off-diagonal (anomalous) components,  $f$  and  $\bar{f}$ , of the



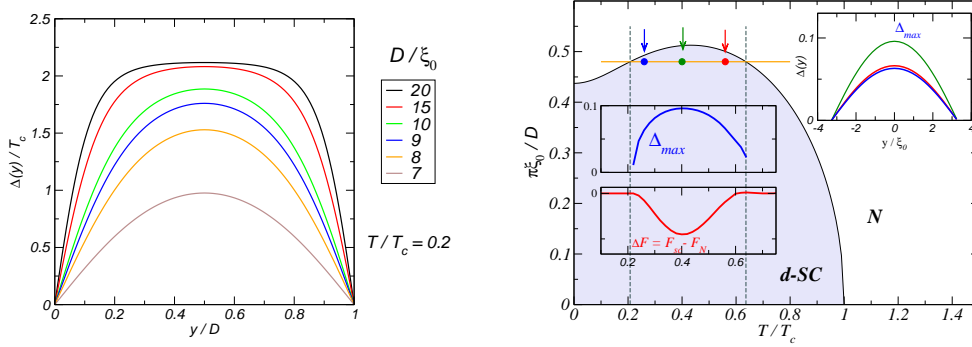


**Figure 4.** The normal-superconducting (N-SC) transition in *d*-wave films. Left: gradual suppression of the order parameter in the film with decreasing thickness  $D$  at fixed temperature. Right: the “temperature-confinement” phase diagram of a *d*-wave film. The N-SC transition line shows re-entrant behavior. The insets present the amplitude of the order parameter and free energy along the line traversing the re-entrance region, and profiles of the order parameter at three points along the line, indicated by the color-coded arrows.

quasiclassical Green’s function are found from the set of equations:

$$\begin{aligned} [\epsilon_m + \frac{1}{2} \mathbf{v}_f \cdot \nabla] f(\mathbf{R}, \mathbf{p}_f; \epsilon_m) &= i g \Delta(\mathbf{R}, \mathbf{p}_f), \\ g^2 - f \bar{f} &= -\pi^2, \quad \bar{f}(\mathbf{R}, \mathbf{p}_f; \epsilon_m) = f(\mathbf{R}, \mathbf{p}_f; -\epsilon_m)^*. \end{aligned} \quad (3.2)$$

Following the step-by-step perturbation scheme one obtains the free energy functional [49]:

$$\begin{aligned} \Delta F &= \sum_{\mathbf{q}} I(T, \mathbf{q}) |\Delta_{\mathbf{q}}|^2 + \frac{1}{2} \sum_{\mathbf{q}_1 + \mathbf{q}_2 = \mathbf{q}_3 + \mathbf{q}_4} K(T, \mathbf{q}_1, \mathbf{q}_2, \mathbf{q}_3, \mathbf{q}_4) \Delta_{\mathbf{q}_1}^* \Delta_{\mathbf{q}_2}^* \Delta_{\mathbf{q}_3} \Delta_{\mathbf{q}_4}, \\ I(T, \mathbf{q}) &= \langle \mathcal{Y}(\mathbf{p}_f)^2 \rangle \ln \frac{T}{T_c} - 2\pi T \sum_{\epsilon_m > 0} \text{Re} \langle \mathcal{Y}^2(\mathbf{p}_f) \left( \frac{1}{\epsilon_m + i\eta_{\mathbf{q}}} - \frac{1}{\epsilon_m} \right) \rangle, \\ K(T, \mathbf{q}_1, \mathbf{q}_2, \mathbf{q}_3, \mathbf{q}_4) &= 2\pi T \sum_{\epsilon_m > 0} \frac{1}{2} \text{Re} \langle \mathcal{Y}^4(\mathbf{p}_f) \frac{\epsilon_m + i(\eta_{\mathbf{q}_1} + \eta_{\mathbf{q}_2} + \eta_{\mathbf{q}_3} + \eta_{\mathbf{q}_4})/4}{(\epsilon_m + i\eta_{\mathbf{q}_1})(\epsilon_m + i\eta_{\mathbf{q}_2})(\epsilon_m + i\eta_{\mathbf{q}_3})(\epsilon_m + i\eta_{\mathbf{q}_4})} \rangle. \end{aligned} \quad (3.3)$$

where  $\eta_{\mathbf{q}} = \frac{1}{2} \mathbf{v}_f \cdot \mathbf{q}$ .

The transition from normal to superconducting state is determined by vanishing quadratic coefficient,  $I(T, \mathbf{q}) = 0$ . If we take a uniform state along the slab the order parameter is vanishing at the specular surfaces  $y = \pm D/2$ , and has the form  $\Delta(y) = \Delta \cos Qy$  with  $Q = \pi/D$ , and the modulating vectors are  $\mathbf{q} = (0, \pm Q)$ . After angle integration over cylindrical Fermi surface,

$$2I(T, \eta = \frac{1}{2} v_f Q) = \ln \frac{T}{T_c} - 2\pi T \sum_{\epsilon_m > 0} \left[ \frac{4\epsilon_m^4}{\eta^4} \left( \sqrt{1 + \frac{\eta^2}{\epsilon_m^2}} - 1 \right)^2 - 1 \right] \frac{1}{\epsilon_m} \quad (3.4)$$

The exact numerical solution for the instability is presented in Fig. 4. At large  $Q$  it has the re-entrant feature, where upon cooling the superconducting order appears and then disappears again into the normal phase. To qualitatively understand this behavior we can take the sum in the limit  $\eta \ll \pi T$ :

$$\Delta F = \frac{1}{2} \Delta^2 \left[ \ln \frac{T}{T_c} + \frac{7\zeta(3)}{8} \tilde{Q}^2 \frac{T_c^2}{T^2} \right] + \mathcal{O}(\Delta^4) \quad (3.5)$$

The temperature-dependent non-local term, arising from the gradient energy, is the one responsible for the re-entrance. At certain fixed  $Q$ , the instability equation  $I(T, \eta) = \ln \frac{T}{T_c} + \frac{7\zeta(3)}{8} \tilde{Q}^2 \frac{T_c^2}{T^2} = 0$  can have two solutions  $T_{high}$  and  $T_{low}$ , that means that at the  $T_{high}$  the negative log term dominates and order parameter appears, but as temperature is lowered, the non-local positive term takes over and superconductivity is suppressed  $T_{low}$ . The order parameter is changing smoothly in this range, and the free energy is lower than that of the normal phase. The approximation  $\xi_0 Q \ll T/T_c$  gives only the qualitative picture; a more careful treatment of the first,  $m = 0$ , non-linear term leads to the same conclusion and allows for more precise determination of the N-SC transition line in the limit  $\tilde{Q} \approx \pi T/T_c$ .

Another explanation of a similar re-entrance feature in a single-component polar state  $\Delta(y)\hat{p}_y$  confined to a slab, was presented in [50]. It was shown that it is a direct consequence of the midgap states and dependence of their energy spectrum on the thickness of the slab.

One of the important features, relevant to the re-entrant N-SC transition, is that the fourth-order coefficient  $K$  is always positive in the region close to the second-order instability. Because of this, the smooth variation of the order parameter with temperature results in a smooth variation of the free energy. The entropy in this temperature range can be less or greater than the normal state's value  $\Delta S(T) = -\partial \Delta F / \partial T$ , but the overall entropy  $S_n(T) + \Delta S(T)$  has positive temperature derivative (positive specific heat), and no thermodynamic inequality is violated in the re-entrant regime. This can be contrasted with back-bending feature of linearized gap equation of paramagnetic depairing, where  $K(T)$  changes sign along N-SC transition line, resulting in a first-order transition at lower temperatures. It was argued that the back-bending feature in that case indicates thermodynamically unstable configuration due to entropy decrease [51].

Further analysis of the free energy in linearized regime reveals that the translation-invariant state in the film is not stable at low temperatures [49]. The state that is realized in constrained geometry is one that carries current and breaks time-reversal symmetry. The OP structure and the free energy of current-carrying state close to the N-SC transition is:

$$\Delta(\mathbf{R}) = \Delta_2 e^{iQ_x x} \cos Q_y y, \quad \Delta F[Q_x] = -\frac{2 I^2(T, \mathbf{Q})}{2(K_1 + 2K_{12})}, \quad (3.6)$$

denoting  $K_1 = K(\mathbf{q}_1, \mathbf{q}_1, \mathbf{q}_1, \mathbf{q}_1)$ ,  $K_{12} = K(\mathbf{q}_1, \mathbf{q}_2, \mathbf{q}_1, \mathbf{q}_2)$ . The other possible state that involves linear combination of order parameters with two opposite wave vectors, or amplitude modulation of the OP, loses in energy to the current-carrying state [49].

The reason for stability of the current-carrying state that breaks time-reversal symmetry is Andreev bound states near pairbreaking surfaces of the film. These states are known to carry paramagnetic current and they result in the lowering of surface energy. One can see this by looking at the free energy difference between a state with superflow  $\mathbf{p}_s$  and time-reversal invariant state,  $p_s = 0$ , expressed in terms of the local density of states:

$$F(\mathbf{R}, \mathbf{p}_s) - F(\mathbf{R}, 0) = -2N_f \int_{-\infty}^{+\infty} \frac{d\epsilon}{2} \left\langle 2T \ln \left[ 2 \cosh \frac{\epsilon}{2T} \right] (N_{\mathbf{p}_s}(\mathbf{R}, \mathbf{p}_f; \epsilon) - N(\mathbf{R}, \mathbf{p}_f; \epsilon)) \right\rangle. \quad (3.7)$$

This expression is valid when the superflow is small, i.e. when pairbreaking effects of the superflow on the order parameter can be neglected. This way the presence of a current is only reflected via the Doppler shift of the energy spectrum:  $N_{\mathbf{p}_s}(\mathbf{R}, \mathbf{p}_f; \epsilon) = N(\mathbf{R}, \mathbf{p}_f; \epsilon - \mathbf{p}_s(\mathbf{R})\mathbf{v}_f)$ .<sup>1</sup>

<sup>1</sup> This form of the free energy can be obtained from the Luttinger-Ward functional, and one can verify that it gives correct expression for local current in terms of the density of states,

$$\begin{aligned} \mathbf{j}_s(\mathbf{R}) &\equiv \frac{\partial F(\mathbf{R}, \mathbf{p}_s)}{\partial \mathbf{p}_s} = 2N_f \int_{-\infty}^{+\infty} \frac{d\epsilon}{2} \left\langle \mathbf{v}_f 2T \ln \left[ 2 \cosh \frac{\epsilon}{2T} \right] \frac{\partial}{\partial \epsilon} N(\mathbf{R}, \mathbf{p}_f; \epsilon - \mathbf{p}_s(\mathbf{R})\mathbf{v}_f) \right\rangle \\ &= -2N_f \int_{-\infty}^{+\infty} \frac{d\epsilon}{2} \tanh \frac{\epsilon}{2T} \langle \mathbf{v}_f N(\mathbf{R}, \mathbf{p}_f; \epsilon - \mathbf{p}_s(\mathbf{R})\mathbf{v}_f) \rangle \end{aligned}$$

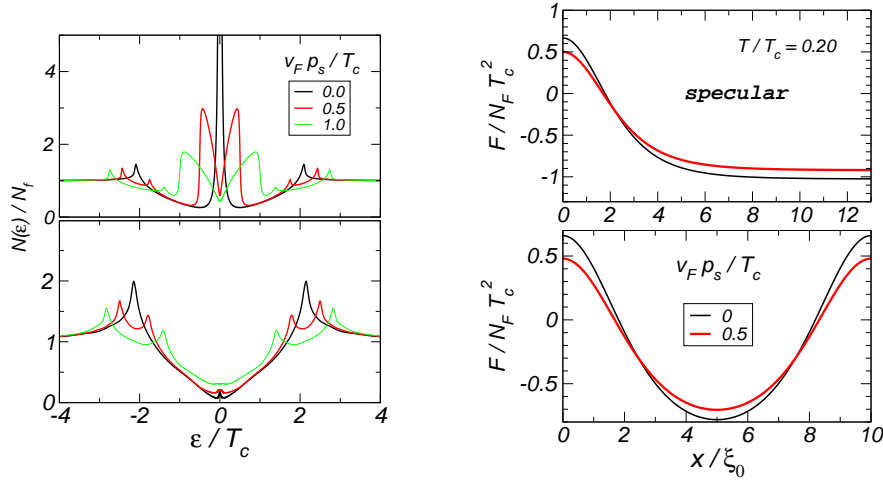


**Figure 5.** Left: density of states in a semi-infinite  $d$ -wave superconductor. The zero-energy peak of Andreev bound states at a specular surface is split by superflow (top left), whereas far away from the surface there is no zero-energy states (bottom left). Right: free energy profile. Bound state splitting lowers free energy at the surface, and continuum states dominate bulk region  $x \gtrsim 4\xi_0$ , increasing free energy (top right). In thin films the surface gain in energy due to split ABS can overcome energy loss in the center (bottom right), favoring current-carrying state.

Surface zero-energy states have delta-function peak with amplitude  $a\Delta_0$ ,  $N_{abs}(\epsilon) = a\Delta_0\delta(\epsilon)$ , and they lower the free energy, when shifted from zero by a superflow  $p_s v_f \gtrsim T$ :

$$\begin{aligned} F_{abs}(\mathbf{R}, \mathbf{p}_s) - F_{abs}(\mathbf{R}, 0) &= -2N_f a \Delta_0 \frac{1}{2} \left\langle 2T \ln \left[ 2 \cosh \frac{\mathbf{p}_s \mathbf{v}_f}{2T} \right] - 2T \ln 2 \right\rangle \\ &\approx -2N_f a \Delta_0 \frac{1}{2} \langle |\mathbf{p}_s \mathbf{v}_f| \rangle = -N_f \frac{2a}{\pi} \Delta_0 p_s v_f \end{aligned} \quad (3.8)$$

- the ABS contribution is linear in the superflow  $p_s$ .

The Doppler-shifted continuum states, on the other hand, result in increase of the local free energy. Assuming that the gap edge  $|\Delta(\mathbf{p}_f)|$  is larger than the Doppler shift, we can make expansion (neglecting possible pairbreaking and non-linear effects from the nodal regions):

$$N(\mathbf{R}, \mathbf{p}_f; \epsilon - \mathbf{p}_s \mathbf{v}_f) - N(\mathbf{R}, \mathbf{p}_f; \epsilon) \approx -\mathbf{p}_s \mathbf{v}_f \frac{\partial N}{\partial \epsilon} + \frac{1}{2} (\mathbf{p}_s \mathbf{v}_f)^2 \frac{\partial^2 N}{\partial \epsilon^2}, \quad (3.9)$$

and take the energy integral in Eq. (3.7). When performing energy integration by parts (two times) one can see that in this case the important role is played by the high-energy parts of the spectrum. The linear  $\mathbf{p}_s \mathbf{v}_f$  term will give zero after Fermi surface average, and the second term gives quadratic in  $p_s$  contribution ( $T = 0$  limit):

$$F_{cont}(\mathbf{R}, \mathbf{p}_s) - F_{cont}(\mathbf{R}, 0) = 2N_f \langle (\mathbf{p}_s \mathbf{v}_f)^2 \rangle = N_f v_f^2 p_s^2. \quad (3.10)$$

As a result, near surfaces zero-energy bound states create favorable conditions for existence of a superflow. The effect of the superflow on local density of states is shown in Fig. 5(left). Quasiclassical calculation of full free energy density is presented in Fig. 5(right). Superflow results in a lower free energy at the surface and higher free energy in the bulk. In thin films, completely dominated by the midgap states, presence of a current lowers total energy.

where in the last step we did integration by parts. This agrees with the usual definition of the current  $\mathbf{j}_s = 2N_f \int_{-\infty}^{+\infty} \frac{d\epsilon}{4\pi i} \langle \mathbf{v}_f g^K \rangle$  after we write the Keldysh propagator in equilibrium as  $g^K = (g^R - g^A) \tanh \frac{\epsilon}{2T} = 2i \text{Im}(g^R) \tanh \frac{\epsilon}{2T} = -2\pi i N_{\mathbf{p}_s}(\mathbf{R}, \mathbf{p}_f; \epsilon) \tanh \frac{\epsilon}{2T}$ .

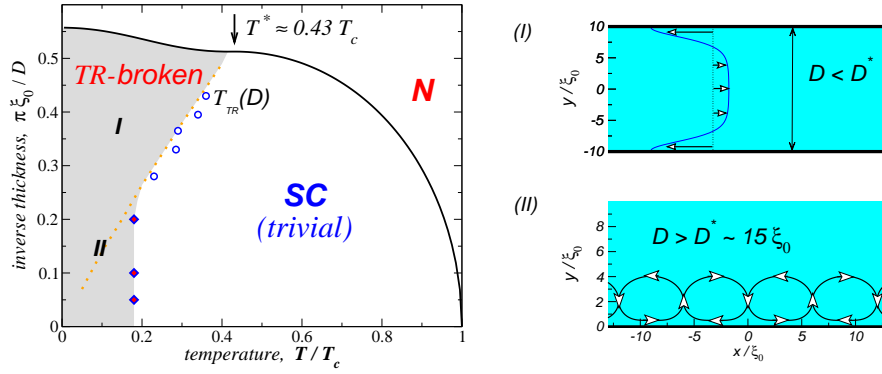


**Figure 6.** Phase diagram of a  $d$ -wave state in film geometry with pairbreaking orientation of the surfaces. In very thin films, surface Andreev states spontaneously split producing a flowing current. In films with  $D \lesssim 15\xi_0$  when states on the two film surface can ‘feel’ each other, the current pattern is linear along the film, and onsets at the dotted line, region I [49] (open circles are from [52]). As the separation between surfaces becomes large, the ABS at a given surface re-arrange themselves and create a circulating current pattern at each surface, diamonds, region II [52].

Phase diagram of  $d$ -wave superconductivity in films is shown in Fig. 6. The trivial superconducting state gives way at low temperature to a state with broken time-reversal symmetry. The structure of the spontaneously generated currents depends on the size of the system. In a small- $D$  sample, non-local interaction of the bound states at different edges of the film, lead to currents parallel to the film surfaces. The superflow in very thin films is uniform in the cross-section of the film,  $p_s(y) = \text{const}$ . The transition temperature  $T_{TR}(D)$  can be estimated in this regime as follows. The free energy has bound state contribution from the boundary regions of size  $L_\xi \sim \xi_0$  and the continuum contribution from the entire width of the film  $D$ :  $F(p_s) - F(0) \approx -N_f \frac{2a}{\pi} \Delta_0 p_s v_f 2L_\xi + N_f p_s^2 v_f^2 D$ . The minimum of free energy is given by superflow  $p_s \propto L_\xi \Delta_0 / v_f D$ , and the transition temperature into the TR-broken state, defined by the splitting of the bound states by this superflow, is  $T_{TR} \approx p_s v_f \propto L_\xi \Delta_0 / D$  - linear in  $1/D$ , dotted line in Fig. 6(left). This line results in  $T_{TR} = 0$  for semi-infinite ‘neutral’ superconductor. In a real, charged superconductors coupling to magnetic field limits the currents to the region of magnetic penetration length  $\lambda$ . The energy balance equation becomes  $F(p_s) - F(0) \approx -N_f (2a/\pi) \Delta_0 p_s L_\xi + N_f p_s^2 v_f^2 \lambda$ , that results in spontaneous surface currents at temperatures below  $T_s \propto (\xi_0/\lambda) T_c$  even in semi-infinite material [12].

However, in samples larger than  $10 - 15\xi_0$ , having a uniform, or even exponentially decaying, superflow away from the edges of the film becomes energetically too costly, and the order parameter adjusts its phase to create a non-uniform two-dimensional pattern of circulating currents limited only to the surface region [52]. The period of the current cell is about the width when the bound states on two surfaces ‘de-couple’ from each other,  $10 - 15\xi_0$ . This indicates that the non-local interactions between bound states is the main driving mechanism for TR-broken state, and the characteristic scale for this interaction is  $10\xi_0$ . The temperature that marks onset of current-circulating state becomes thickness-independent, as a result, shown by diamonds in phase diagram, Fig. 6(left).

### (b) Multi-component superfluids

In superfluids that have multiple order parameter components, structure of the bound states at interfaces is more intricate. Various components of the order parameter suppressed differently at the boundaries, depending on their momentum space basis functions, and the non-linear coupling between components can transfer weight between them. This interplay creates new ways of

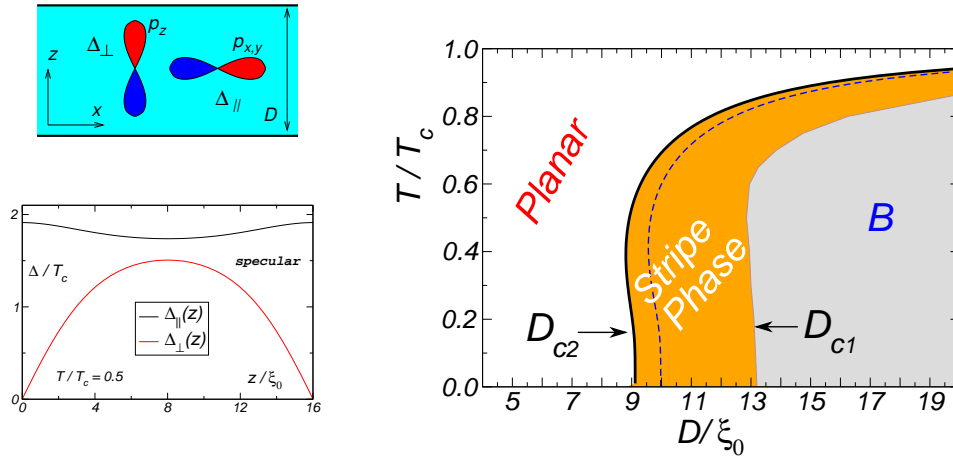


**Figure 7.** Left: Superfluid  $^3\text{He}$  confined to a slab or a film. Order parameter component that depends on  $\hat{p}_z$ -momentum gets suppressed, while ‘parallel’ orbitals result in surface enhancement of corresponding components (specular reflection). Right: transition from the distorted B-phase into Planar phase (weak coupling) occurs through a phase that breaks translational invariance along the plane of the film, and forms periodic structure with period of several  $\xi_0$ . [53]

adjusting the OP structure in confined geometry, and shifting to a new non-trivial minima in multi-dimensional energy landscape.

In spin-1  $p$ -wave superfluid  $^3\text{He}$  the vector order parameter is parametrized by  $3 \times 3$  matrix,

$$\Delta_\alpha(\mathbf{R}, \mathbf{p}_f) = \sum_{i=x,y,z} A_{\alpha i}(\mathbf{R}) \hat{p}_i, \quad A_{\alpha i} = \begin{pmatrix} A_{xx} & A_{xy} & A_{xz} \\ A_{yx} & A_{yy} & A_{yz} \\ A_{zx} & A_{zy} & A_{zz} \end{pmatrix} \quad (3.11)$$

that gives the momentum dependence in terms of orbitals  $(\hat{p}_x, \hat{p}_y, \hat{p}_z)$ . Scattering of the quasiparticles off the  $xy$ -plane, for example, suppresses the orbital- $\hat{p}_z$  OP components  $A_{\alpha z}$  for specular scattering and all components for diffuse scattering. Neglecting the dipole-dipole interaction that orients the spin vector relative to the orbital vector in a certain way, the stable phase in thick films is the distorted B-phase where OP components depend only on the transverse coordinate, which traditionally is denoted  $z$  (rather than  $y$  as was in the case of 2D superconductor):

$$A_{\alpha i}(\mathbf{R})_B = \begin{pmatrix} \Delta_\parallel(z) & 0 & 0 \\ 0 & \Delta_\parallel(z) & 0 \\ 0 & 0 & \Delta_\perp(z) \end{pmatrix} \quad (3.12)$$

The transverse  $\Delta_\perp(0) = \Delta_\perp(D) = 0$  component is pinned by the boundary conditions and gets suppressed as film is made thinner, vanishing at a second-order transition into Planar phase (weak coupling)

$$A_{\alpha i}(\mathbf{R})_P = \begin{pmatrix} \Delta_\parallel^0 & 0 & 0 \\ 0 & \Delta_\parallel^0 & 0 \\ 0 & 0 & 0 \end{pmatrix} \quad (3.13)$$

where only  $z$ -independent parallel components  $\Delta_\parallel^0$  remain that do not get suppressed by specular scattering. This transition is shown by dashed line in Fig. 7, and also features back-bending behavior at low  $T$ .

It has been predicted [53] that in weak coupling in the vicinity of this transition, the superfluid with order parameter  $A_{\alpha i}(z)$ , translationally invariant along the film’s plane, is unstable towards formation of a new phase that spontaneously breaks this symmetry and generates longitudinal

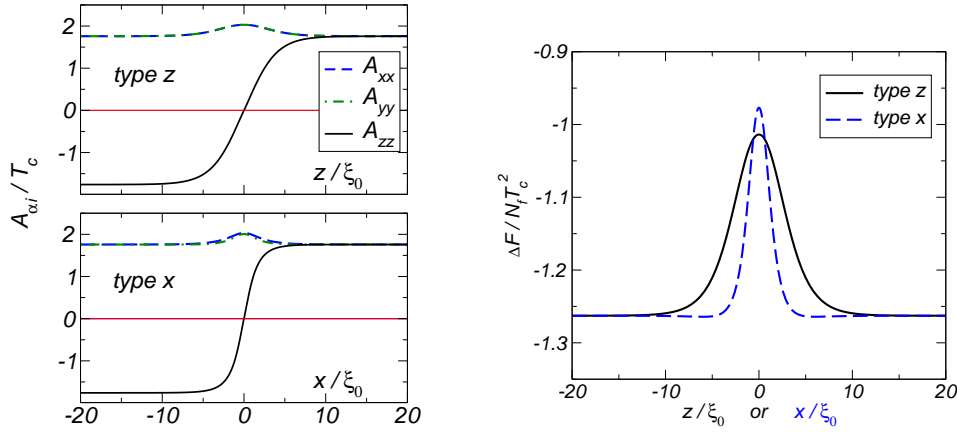


**Figure 8.** Left: order parameter in domain walls of the B-phase [56]. These configuration of the OP suppression are not stable in the bulk, but can naturally appear and compete in confined geometry to lower free energy. Right: the free energy profile associated with the domain walls. The longitudinal, type-x, wall is narrower and costs less energy.

modulations of the order parameter  $A_{\alpha i}(z, x)$ , forming stripes along some direction in the plane of the film.

The stability and structure of this phase is a consequence of multiple inhomogeneous configurations in multi-component superfluids. The two relevant configurations for superfluid  $^3\text{He}$  are shown in Fig. 8. Suppression of the transverse component  $A_{zz}(z) = \Delta_{\perp}(z)$  at a pairbreaking surface can be mapped onto a domain wall in infinite space where this component changes sign  $\Delta_{\perp}(z = \pm\infty) = \pm\Delta_{0B}$ . This domain wall configuration, which we may call type-z, should be compared with another configuration, type-x, when  $A_{zz}$  component of the order parameter changes along the plane of (a very thick, we can imagine) film. The latter configuration costs less in terms of free energy, see Fig. 8 (right) and is, in fact, the lowest energy domain wall configuration [54]. Although such states are not topologically stable in the bulk [54,55], pairbreaking geometry creates environment where such configurations can appear to minimize the total energy in a finite volume. The spectrum of the bound states reflects this interplay, and for the two shown domain wall configurations is presented in Fig. 2.

In the film geometry, the trivial suppression of the  $A_{zz}(z)$  across the film is due to reflection  $\hat{p}_z \rightarrow -\hat{p}_z$ . This loss of condensation energy, similar to that of type-z domain wall, can be reduced by creating additional, type-x, modulation along the film,  $A_{zz}(z, x)$ , shown in top left panel of Fig. 9. This extra modulation ‘undoes’ the trivial pairbreaking by having amplitude sign-change  $A_{zz}(x > 0) \rightarrow -A_{zz}(x < 0)$  along a trajectory that ‘bounces’ off the film surface near  $x = 0$ . The reduction of the pairbreaking appears as energy gains at the T-intersections, shown in bottom left panel of Fig. 9. In sufficiently thin films this energy gain is enough to overcome the extra cost of creating the type-x domain wall across the width of the film. This energy balance determines the  $D_{c1}$  transition in Fig. 7, where a single domain wall enters previously translationally invariant film. The exact structure of the domain wall is described in [53]:  $A_{zz}$  component acquires x-modulation, as we just described, and at the same time a large  $A_{xz}$  OP component also appears.

In Fig. 9, on the right, we can see how the density of states changes with the introduction of such a domain wall. Most of the weight redistribution is associated with the midgap states. As we move into the domain wall region along the center of the film, states from the continuum,  $\epsilon \sim \Delta_{0B}$ , move into the gap region  $0.5\Delta_{0B} \lesssim \epsilon \lesssim \Delta_{0B}$ . On the other hand, near the film edges, the low energy bound states shift towards  $\Delta_{0B}$ .

To conclude this discussion, we now find the instability  $D_{c2}$  from the Planar phase into the stripe phase, and show that the emergent new order parameter structure at the transition

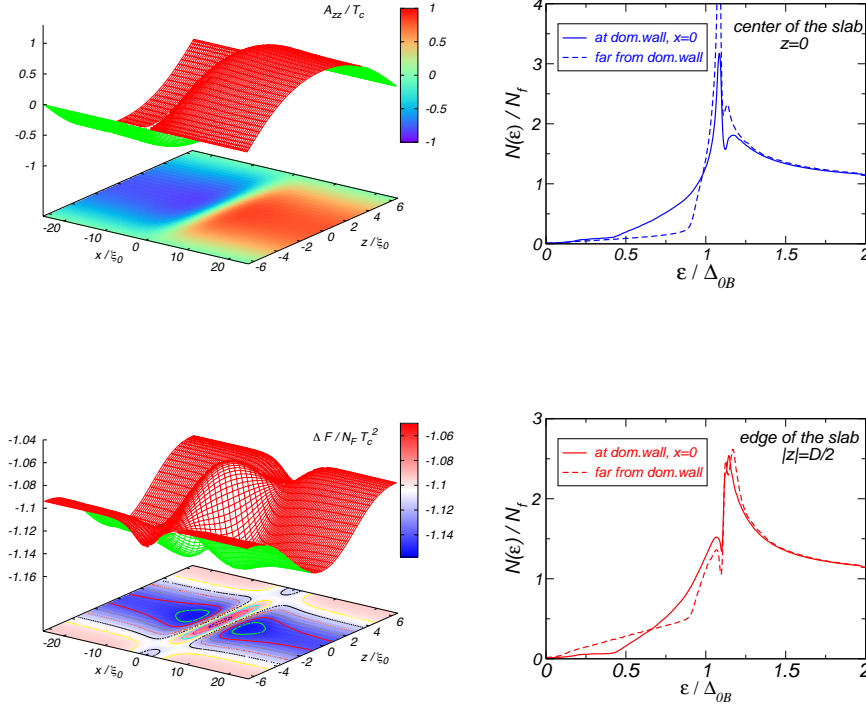


**Figure 9.** Top left: pairbreaking associated with the suppression of the  $A_{zz}(z) = \Delta_{\perp}(z)$  component can be reduced by placing additional (domain wall) modulation in the film  $A_{zz}(x, z)$ . The free energy profile (bottom left) shows energy gain at the edges and the center of the film around this domain wall. Panels on the right show spectral weights far from the domain wall (dashed lines) and at the domain wall  $x = 0$  (solid lines). In the center of the film (top right) the states from continuum move to lower energies, and at the edges (bottom right) low-energy states shift up, as one approaches domain wall at  $x = 0$ .

agrees with the one that appears at the single domain wall transition  $D_{c1}$ . The second-order  $D_{c2}$  instability is defined as the lowest  $D$  line where new OP structure, different from Planar background phase, emerges. We will see that the main difference between this Planar-B transition in superfluid  $^3\text{He}$  and the N-SC transition in a single-component superconductor, is that the existing background condensate  $^3\text{He}$  film create coupling between the newly generated OP components, enforcing certain restrictions on the possible structure of the emergent state, even before the fourth order GL terms are compared for various phases.

The procedure to find the instability is to find non-trivial self-consistent solution for the order parameter to linear order in perturbation,  $\hat{\Delta}_0(\mathbf{R}, \mathbf{p}_f) + \hat{\Delta}_1(\mathbf{R}, \mathbf{p}_f)$ . The unperturbed phase is the Planar state with order parameter  $\Delta_0(\mathbf{R}, \mathbf{p}_f) = (\Delta_{\parallel}^0 \hat{p}_x, \Delta_{\parallel}^0 \hat{p}_x, 0)$  and the Green's function:

$$\hat{f}_0 = \pi \frac{\Delta_0}{\sqrt{\epsilon_m^2 + |\Delta_0|^2}} (i\sigma\sigma_y), \quad \hat{g}_0 = -\pi \frac{i\epsilon_m}{\sqrt{\epsilon_m^2 + |\Delta_0|^2}}. \quad (3.14)$$

The self-consistency equation for the linear correction to the order parameter  $\Delta_{1,\alpha}(\mathbf{R}, \mathbf{p}_f) = a_{\alpha i}(\mathbf{R}) \hat{p}_i$  is,

$$a_{\alpha i}(\mathbf{R}) \ln \frac{T}{T_c} = T \sum_{\epsilon_m} 3 \int \frac{d\Omega_{\hat{\mathbf{p}}}}{4\pi} \hat{p}_i \left( f_{1,\alpha}(\mathbf{R}, \mathbf{p}_f; \epsilon_m) - \frac{a_{\alpha j}(\mathbf{R}) \hat{p}_j}{|\epsilon_m|} \right). \quad (3.15)$$



Linear order correction  $f_{1,\alpha}$  to the off-diagonal propagator is found from Eilenberger equations and normalization conditions, for  $\hat{g}$  and  $\hat{f}$  components. Breaking the commutator in (2.1) into components we have

$$\begin{aligned} i\mathbf{v}_f \cdot \nabla \hat{g} + (-\hat{\Delta} \hat{f} + \hat{f} \hat{\Delta}) &= 0, & \hat{g}^2 + \hat{f} \hat{f} &= -\pi^2, \\ i\mathbf{v}_f \cdot \nabla \hat{f} + 2i\epsilon_m \hat{f} + (-\hat{\Delta} \hat{g} + \hat{g} \hat{\Delta}) &= 0, & \hat{g} \hat{f} + \hat{f} \hat{g} &= 0. \end{aligned} \quad (3.16)$$

We linearize them with respect to  $(\hat{g}_1, \hat{f}_1, \hat{\Delta}_1)$ , and in the normalization conditions we use expressions for the background Green's functions (3.14) together with symmetry relations (2.3):

$$\begin{aligned} (2i\epsilon_m + i\mathbf{v}_f \cdot \nabla) \hat{f}_1 + (-\hat{\Delta}_0 \hat{g}_1 + \hat{g}_1 \hat{\Delta}_0) &= \hat{\Delta}_1 \hat{g}_0 - \hat{g}_0 \hat{\Delta}_1, & \hat{g}_1 \hat{\Delta}_0 + \hat{\Delta}_0 \hat{g}_1 &= 0 \\ i\mathbf{v}_f \cdot \nabla \hat{g}_1 + (-\hat{\Delta}_0 \hat{f}_1 + \hat{f}_1 \hat{\Delta}_0) &= (\hat{\Delta}_1 \hat{f}_0 - \hat{f}_0 \hat{\Delta}_1), & -2i\epsilon_m \hat{g}_1 + \hat{f}_1 \hat{\Delta}_0 + \hat{\Delta}_0 \hat{f}_1 &= 0 \end{aligned} \quad (3.17)$$

Here we treat the gradient terms non-perturbatively, assuming they have same magnitude as the other energy terms. Combining pairs of equation in each line we eliminate  $\hat{g}_1$  and  $\hat{f}_1$ :

$$\begin{aligned} \left( i\epsilon_m + \frac{i}{2} \mathbf{v}_f \cdot \nabla \right) \hat{f}_1 + \hat{g}_1 \hat{\Delta}_0 &= -\hat{g}_0 \hat{\Delta}_1, \\ \left( -i\epsilon_m + \frac{i}{2} \mathbf{v}_f \cdot \nabla \right) \hat{g}_1 + \hat{f}_1 \hat{\Delta}_0 &= \frac{1}{2} (\hat{\Delta}_1 \hat{f}_0 - \hat{f}_0 \hat{\Delta}_1). \end{aligned} \quad (3.18)$$

Using the fact the unperturbed solution is uniform,  $\nabla_{\mathbf{R}} \hat{g}_0 = 0$ , we can use the second equation to eliminate  $\hat{g}_1$  from the first,

$$\begin{aligned} \left( -i\epsilon_m + \frac{i}{2} \mathbf{v}_f \cdot \nabla \right) \left( i\epsilon_m + \frac{i}{2} \mathbf{v}_f \cdot \nabla \right) \hat{f}_1 + \left( -\hat{f}_1 \hat{\Delta}_0 + \frac{\hat{\Delta}_1 \hat{f}_0 - \hat{f}_0 \hat{\Delta}_1}{2} \right) \hat{\Delta}_0 \\ = -\hat{g}_0 \left( -i\epsilon_m + \frac{i}{2} \mathbf{v}_f \cdot \nabla \right) \hat{\Delta}_1 \end{aligned} \quad (3.19)$$

Substituting unitarity condition  $\hat{\Delta}_0 \hat{\Delta}_0 = -|\Delta_0|^2$ , and expressions for  $\hat{g}_0, \hat{f}_0$ , one derives final equation for corrections to propagator, linear in order parameter deviations,

$$\begin{aligned} \left[ \epsilon_m^2 + |\Delta_0|^2 + \left( \frac{i}{2} \mathbf{v}_f \cdot \nabla \right)^2 \right] \hat{f}_1 &= \frac{\pi}{\sqrt{\epsilon_m^2 + |\Delta_0|^2}} \\ &\times \left[ i\epsilon_m \left( -i\epsilon_m + \frac{i}{2} \mathbf{v}_f \cdot \nabla \right) \hat{\Delta}_1 + \frac{1}{2} (|\Delta_0|^2 \hat{\Delta}_1 + \hat{\Delta}_0 \hat{\Delta}_1 \hat{\Delta}_0) \right]. \end{aligned} \quad (3.20)$$

The gradient term on the right-hand side acting on the order parameter can be dropped since it is odd in energy and will disappear after  $\pm\epsilon_m$  energy summation in the self-consistency equation. Equation for the off-diagonal vector  $\mathbf{f}_1(\mathbf{R}, \mathbf{p}_f; \epsilon_m)$  in terms of the order parameter  $\Delta_1(\mathbf{R}, \mathbf{p}_f)$ ,

$$\left[ \epsilon_m^2 + |\Delta_0|^2 + \left( \frac{i}{2} \mathbf{v}_f \cdot \nabla \right)^2 \right] \mathbf{f}_1 = \pi \frac{\left[ \epsilon_m^2 + \frac{1}{2} |\Delta_0|^2 \right] \Delta_1 - \Delta_0 (\Delta_0 \Delta_1^*) + \frac{1}{2} (\Delta_0^2) \Delta_1^*}{\sqrt{\epsilon_m^2 + |\Delta_0|^2}} \quad (3.21)$$

couples, through finite  $\Delta_0$ , solutions for  $\Delta_1$  and its complex conjugate  $\Delta_1^*$ . As a result, spatially dependent  $e^{\pm i\mathbf{q}\mathbf{R}}$  solutions exist in pairs and a current-carrying solution is not possible. We use Fourier expansion to solve for  $\mathbf{f}_1$  in terms of OP harmonics:

$$a_{\alpha i}(\mathbf{R}) = \sum_{\mathbf{q}} a_{\alpha i}(\mathbf{q}) e^{i\mathbf{q}\mathbf{R}} \quad \Rightarrow \quad f_{1,\alpha}(\mathbf{R}, \mathbf{p}_f; \epsilon_m) = \sum_{\mathbf{q}} f_{1,\alpha}(\mathbf{q}, \mathbf{p}_f; \epsilon_m) e^{i\mathbf{q}\mathbf{R}} \quad (3.22)$$

and write coupled self-consistency equations for the pairs  $a_{\alpha i}(\mathbf{q})$  and  $a_{\alpha i}(-\mathbf{q})^*$ ,

$$\ln \frac{T}{T_c} \begin{pmatrix} a_{\alpha i}(\mathbf{q}) \\ a_{\alpha i}(-\mathbf{q})^* \end{pmatrix} = \begin{pmatrix} K_{ij}^{\alpha\beta}(\mathbf{q}, \mathbf{q}) & K_{ij}^{\alpha\beta}(\mathbf{q}, -\mathbf{q}) \\ K_{ij}^{\alpha\beta}(\mathbf{q}, -\mathbf{q})^* & K_{ij}^{\alpha\beta}(\mathbf{q}, \mathbf{q}) \end{pmatrix} \begin{pmatrix} a_{\beta j}(\mathbf{q}) \\ a_{\beta j}(-\mathbf{q})^* \end{pmatrix} \quad (3.23)$$

where the  $a$ -columns consist of 18 complex numbers, and the  $K$ -matrix is  $18 \times 18$ . Its elements are,

$$\begin{aligned} K_{ij}^{\alpha\beta}(\mathbf{q}, \mathbf{q}) &= 2\pi T \sum_{\epsilon_m > 0} 3 \int \frac{d\Omega_{\mathbf{p}_f}}{4\pi} \hat{p}_i \hat{p}_j \left[ \left( \frac{E_m}{E_m^2(\mathbf{q})} - \frac{1}{\epsilon_m} \right) - \frac{|\Delta_0(\mathbf{p}_f)|^2}{2E_m E_m^2(\mathbf{q})} \right] \delta_{\alpha\beta}, \\ K_{ij}^{\alpha\beta}(\mathbf{q}, -\mathbf{q}) &= 2\pi T \sum_{\epsilon_m > 0} 3 \int \frac{d\Omega_{\mathbf{p}_f}}{4\pi} \hat{p}_i \hat{p}_j \frac{1}{E_m E_m^2(\mathbf{q})} \left[ \frac{1}{2} \Delta_0(\mathbf{p}_f)^2 \delta_{\alpha\beta} - \Delta_0(\mathbf{p}_f)_\alpha \Delta_0(\mathbf{p}_f)_\beta \right], \end{aligned} \quad (3.24)$$

where shorthand  $E_m = \sqrt{\epsilon_m^2 + |\Delta_0(\mathbf{p}_f)|^2}$  and  $E_m(\mathbf{q}) = \sqrt{\epsilon_m^2 + |\Delta_0(\mathbf{p}_f)|^2 + (\frac{1}{2}\mathbf{v}_f \mathbf{q})^2}$  are used. The  $K$ -matrix is Hermitian and we numerically find all non-trivial solutions to Eq. (3.23). At a given  $T$  we vary  $q_x$  to find maximal  $q_z$  that satisfies  $|\hat{K}(T, q_x, q_z) - \hat{1} \ln(T/T_c)| = 0$ , and find the eigenvector  $(a_{\alpha i}(\mathbf{q}), a_{\alpha i}(-\mathbf{q})^*)$  for the pairs  $(q_x, q_z)$ . We will then impose a boundary condition that all components with  $\hat{p}_z$  orbital dependence vanish at the specular edges of the slab for any  $x$ :

$$a_{\alpha z}(x, z = \pm D/2) = \sum_{q_z, q_x} a_{\alpha z}(\mathbf{q}) e^{i(q_z D/2 + q_x x)} = 0. \quad (3.25)$$

This procedure determines the transition values of the wave vector, which we denote by capital letters  $Q_z(T)$  and  $Q_x(T)$ , and the structure of the nucleating order parameter at the transition. For transition from the Planar phase, we find two degenerate solutions (due to  $z$ -reflection symmetry) given by pair  $(a_{\alpha i}(\mathbf{Q}_1), a_{\alpha i}(-\mathbf{Q}_1)) = \{-a_{zx}, a_{zz}\}$  with  $\mathbf{Q}_1 = (Q_x, Q_z)$ , and pair  $(a_{\alpha i}(\mathbf{Q}_2), a_{\alpha i}(-\mathbf{Q}_2)) = \{a_{zx}, a_{zz}\}$  with  $\mathbf{Q}_2 = (Q_x, -Q_z)$ . The (real) components of the eigenvectors have amplitudes  $a_{zz} = 1$ ,  $a_{zx} \approx 0.6$  in the temperature range  $0.2 < T/T_c < 0.6$ . The two are different by the relative sign between the  $a_{zx}$  and  $a_{zz}$  components, as a result of  $Q_z$  inversion. These two solutions describe transition from the Planar state into a new state:

$$A_{\alpha i}^{(0)} = \Delta_0 \begin{pmatrix} 1 & 0 & 0 \\ 0 & 1 & 0 \\ 0 & 0 & 0 \end{pmatrix} \implies A_{\alpha i}^{(0)} + a_{\alpha i}(\mathbf{R})_{\mathbf{Q}_1} + a_{\alpha i}(\mathbf{R})_{\mathbf{Q}_2} \quad (3.26)$$

with the structure of the nucleated order parameter,

$$a_{\alpha i}(\mathbf{R})_{\mathbf{Q}_1} = \Delta_1 \begin{pmatrix} 0 & 0 & 0 \\ 0 & 0 & 0 \\ -a_{zx} & 0 & a_{zz} \end{pmatrix} \left( e^{i(Q_z z + Q_x x)} + e^{-i(Q_z z + Q_x x)} \right), \quad (3.27)$$

$$a_{\alpha i}(\mathbf{R})_{\mathbf{Q}_2} = \Delta_2 \begin{pmatrix} 0 & 0 & 0 \\ 0 & 0 & 0 \\ a_{zx} & 0 & a_{zz} \end{pmatrix} \left( e^{i(-Q_z z + Q_x x)} + e^{-i(-Q_z z + Q_x x)} \right). \quad (3.28)$$

To satisfy the boundary condition  $a_{zz}(x, z = \pm D)$  the total solution must be a combination of these two, with equal amplitudes  $\Delta_1 = \Delta_2$ , so that

$$a_{\alpha i}(\mathbf{R}) = a_{\alpha i}(\mathbf{R})_{\mathbf{Q}_1} + a_{\alpha i}(\mathbf{R})_{\mathbf{Q}_2} = \Delta' \begin{pmatrix} 0 & 0 & 0 \\ 0 & 0 & 0 \\ a_{zx} \sin Q_z z \sin Q_x x & 0 & a_{zz} \cos Q_z z \cos Q_x x \end{pmatrix} \quad (3.29)$$

and the boundary condition  $\cos Q_z D/2 = 0$  giving the smallest film thickness for maximal  $Q_z$ ,

$$D = \frac{\pi}{Q_z}. \quad (3.30)$$

This structure agrees with the order parameter obtained numerically in [53]. Note, that any other eigenmodes would have lower  $Q_z$  and would give transition in thicker films; also the opposite choice for the relative overall sign between  $\mathbf{Q}_1, \mathbf{Q}_2$  solutions,  $\Delta_1 = -\Delta_2$ , would give  $A_{zz} \sim \pm \sin Q_z D/2 = 0$ , which would again lead to a thicker film,  $D = 2\pi/Q_z$ .

### (c) Other geometries, pairing states, and effects of competing interactions and boundary conditions

From the two cases above, we see that the structure and stability of new phases in confined geometry depends on the symmetry and number of OP components. Any interaction that creates additional energy shifts of the midgap states, modify their weights, and affects OP suppression, will have a significant effect on the free energy landscape and appearance of new phases.

For example in the  $d$ -wave films, the structure of the non-uniform states that is generated in the films is determined by the  $1/(\epsilon_m - \mathbf{q}\mathbf{v}_f/2)$  factors in Eqs. (3.3), that can be interpreted as Doppler-shifted quasiparticles' energy due to non-uniform order parameter. This shift will be strongly affected by any changes in the Fermi surface shape through direction of Fermi velocity  $\mathbf{v}_f$  and the anisotropy of the density of states that appear in the FS angle integrals. Work [57] demonstrated that if the Fermi surface has square shape with flat nested regions and the  $d$ -wave nodes residing on its sharp ends, the broken time-reversal state is stabilized in a much thinner films.

Similar energy shifts occur when there is applied magnetic field. In a case of Zeeman interaction between external field  $H$  and electron spin moment, the shifts are isotropic in momentum space  $1/(\epsilon_m - \mathbf{q}\mathbf{v}_f/2 \pm \mu_B H)$ , which creates interplay between non-uniform effects and Pauli-breaking effects, resulting in rich phase diagram that features re-entrant superconductivity [58].

Random scattering effects, either by impurities, and in particular by the atomically rough surfaces, are known to deform the spectrum of midgap states in a significant way. Calculations have shown, however, that the spontaneous current-carrying state is relatively robust toward scattering. For example, to completely suppress this state, impurity concentrations that give mean free path  $\ell/\xi_0 \sim 5$  and 60%  $T_c$  suppression, are needed [49]. A calculation [59] with continuously adjusted surface specularity parameter  $S$  has shown that the current-carrying state is suppressed when specular reflection probability is  $S \lesssim 0.2$  - very close to diffuse limit  $S = 0$ . Re-orientation of the crystal axes relative to the surface plane,  $\mathcal{Y}(\phi) = \sin 2(\phi - \phi_0)$ , reduces phase space for trajectories that produce zero-energy states. To eliminate spontaneous currents misalignment angles  $\phi_0 \sim 23^\circ$ , that reduce the weight of zero-energy states in about half, are required [52].

In multi-component systems, a phase with broken continuous translations has been described in  $^3\text{He-B}$ , confined to narrow cylinders. [20] Recent work by Northwestern University theory group, has shown that in Ginzburg-Landau regime the strong-coupling effects in  $^3\text{He}$  do not eliminate the stripe state in film geometry. They also have discovered that a similar instability towards formation of periodic order in two-dimensional strips of chiral  $p$ -wave state  $\Delta_x \hat{p}_x + i\Delta_y \hat{p}_y$ .

## 4. Experimental investigation of thin films

It has been realized very early that Andreev bound states and spontaneous surface currents can help determine symmetry and structure of the order parameter in new superconductors. Their properties have been studied and used in high- $T_c$  materials, in particular in tunneling experiments [60,61]. Most of the work concentrated on description of subdominant pairing channels, as a way of identifying the symmetry and origin of the pairing state in cuprates, since unusual surface properties can give clear signature of such pairing states. [62–65]

In superfluid  $^3\text{He}$ , that has one of the most complex order parameter structures out of all known superconductors, investigation of Andreev surface states is particularly interesting. Despite extensive work, up to date there have been few experiments directly testing their presence. Measurement of transverse impedance in a series of experiment [66–68] demonstrated importance of surface states for mechanical coupling between the transducers and the oscillations of the liquid, and determined their signatures for varying surface roughness. Specific heat

measurements of superfluid  $^3\text{He}$  in silver heat exchanger constructed of sintered silver particles looked at thermodynamic properties of the Andreev states. [69]

Small scale devices, where pairbreaking and bound states dominate physical properties, provide a unique aspect for investigation of unconventional superfluid and superconducting phases, and can provide valuable insight into properties of the surface bound states themselves. While film geometry in superconductors can be considered unusual, superfluid  $^3\text{He}$  provides a more natural ground for investigation of complex condensates in restricted geometries, such as films or slabs. For this reason experimental investigation of superfluid  $^3\text{He}$  phases in slabs or films has started early, following theoretical development in 1970-80s.

After detection in 1985 of superfluidity in thin  $^3\text{He}$  films formed on vertical walls [70], a number of different techniques was applied to study their properties. A film formed on an elevated substrate [71] was used to measure suppression of the superfluid transition temperature, and flow properties. Critical current, superfluid density were measured by flow over beaker rim [72,73]. Torsional oscillators [74] were used to determine  $T_c(D)$  dependence, and superfluid density. An innovative way to excite and detect third sound waves in superfluid films was used in [75]. Another dynamical excitation method by inter-digitated capacitors was employed to study flow in films [76–78].

Phase transitions between  $^3\text{He}$  phases in confinement, driven by OP suppression, is typically investigated using pressure dependence of the coherence length  $\xi_0(p)$  that changes from 77 nm at zero pressure to 15 nm at the melting pressure, making it possible for manipulation of effective film thickness  $D/\xi_0(p)$  through pressure variation. NMR measurements in stacks of Mylar sheets reported measurements of superfluid density and identified the thin-film phase to be the A-phase in  $0.3\text{ }\mu\text{m}$  slabs [79]. Measurements [80] reported A-B transition in a stack of slabs with distribution of thickness from around 0 to  $\sim 1.5\text{ }\mu\text{m}$ . The pressure dependence of A-B transition was also investigated in [81] using more uniformly separated polyethylene films of  $1.1 \pm 0.3\text{ }\mu\text{m}$ . In a similar experiment the A-B transition was mapped in  $0.8 \pm 0.04\text{ }\mu\text{m}$  as a function of pressure [82].

The last decade saw several significant advances on the experimental side. The techniques were developed for more precise nano-fabrication that promise a better look at the underlying physics of confined superfluids. Several different types of experimental cells have been developed with the goal of studying of superfluid in a single slab. Single-film devices allow for better control of uniform thickness. Due to precisely defined geometry and dimensions single-film cells have better ability to investigate ABS, and they can also be manufactured with purpose of dynamical excitation of surface ABS. Royal Holloway University of London group pioneered new ways to fabricate single-slab nanofluidic cavity and to perform high-sensitivity NMR measurements in a small-volume systems and measured  $T_c$  suppression and A-B transition [83,84]. The team at University of Florida built micro-electro-mechanical systems (MEMS) oscillators that can dynamically excite quasiparticles in thin films [85–87]. The low-temperature group at University of Alberta produced and started testing nano-mechanical resonator [88]. These techniques are well-suited to explore whether there is evidence of new unusual phases, and to advance our understanding of properties of the surface states and superfluid phases in confinement, where several discrepancies between theory and experiment persist and need to be resolved.

Suppression of the critical temperature of superfluid,  $T_c(D)$ , due to diffuse surface scattering is potentially one of these anomalies. The earlier flow [72,73] and torsion oscillator [74] measurements had large error bars that agreed reasonably well with theoretical prediction of suppression [16]. A more recent data of two different groups [76,83] show noticeable deviations from theoretical predictions and surprisingly larger than expected suppression in both low and high temperature regimes. A more detailed description of some of the experiments is summarized in Fig. 10 of [84].

There is also no consistency between various theoretical and experimental conclusions about the confinement-induced A-B transition. In very thin slabs  $0.3\text{ }\mu\text{m}$  experiment [79] did not observe the AB transition where it was expected from GL theory [17] calculations. Later experiments

[80,82] saw this transition and concluded that its approximate location is in agreement with calculations based on variational approach [89], but found that  $^4\text{He}$  coverage and change from diffuse to specular quasiparticle scattering moved the AB transition line to higher temperature, in disagreement with GL and QC theory. The most recent experiment in a high-precision single cell [83] showed significantly lower  $T_{AB}$  than predicted by weak-coupling quasiclassical calculations, but saw  $T_{AB}^{\text{specular}} < T_{AB}^{\text{diffuse}}$  in agreement with quasiclassical theory prediction [30].

Several other anomalies have been seen in transport experiments. Magnitude of the critical current in [72,73] was significantly smaller than expected from early theoretical models, and flow rate transition was observed in [73]. Superfluid density in torsional oscillator [74] showed anomaly and some sort of transition when films became  $D \lesssim 275$  nm. Third sound oscillation modes in  $^3\text{He}$  films [75] show unusual mode coupling. Film flow studies [76–78] reported two regimes of superflow dissipation in films with  $D$  below and above  $1\mu\text{m}$ .

These all call for deeper and wide-ranging investigation of states in films and slabs, to fully understand theoretical models and physical properties of phases in confinement.

## 5. Conclusion

Unconventional superconductors and superfluids provide an excellent testing ground of our understanding of complex pairing condensates with multiple spontaneously broken symmetries. One of the special signatures of these states is extreme sensitivity of quasiparticle states to Andreev particle-hole scattering on interfaces that leads to formation of low-energy bound states concentrated in the region of several coherence length  $\xi_0$  near interface.

These states carry information about structure of the underlying order parameter and their properties, such as dispersion, weight, spin structure etc, encode the way these states were created: relative orientation of the interface with respect to the crystal lattice, scattering properties of a surface, or a particular way the incoming and outgoing trajectories connect the points of momentum-space Hamiltonian.

Due to presence of midgap bound states and order parameter suppression, the surface region can have very different experimental signatures from those of the bulk phase. In confined geometry, influence of surface Andreev states is greatly enhanced because smallness of the volume precludes formation of dominant bulk phases. As a result, a new part of the condensate's phase space can be explored. Beside configurations that are trivially modified versions of the bulk states, several new phases are expected to be the ground states in confined geometry. The new phases have different symmetry properties, that depend on the nature of the pairing interaction. In single-component  $d$ -wave film spontaneous currents appear, breaking time-reversal symmetry. The currents are generated due to the fact that the bound states can lower their energy in the presence of a superflow. In superfluid  $^3\text{He}$  multi-component nature of the condensate results in the amplitude modulation of the order parameter in the plane of the film, breaking continuous translation symmetry.

Recent experimental progress in manufacturing of nanometer-scale cells promise a new window into extreme regimes of confinement, and a new approach to investigation of properties of surface bound states and unconventional condensates. Superfluid  $^3\text{He}$  in confinement is a particularly interesting system where multiple phenomena challenge our understanding, both experimentally and theoretically. One question is whether or not additional phases may be stabilized depending on the geometry and surface structure of the confining geometry. So far there seems to be no experimental evidence for the proposed stripe phase in  $^3\text{He}$  films. Detection of the non-uniform superconducting states, however, is a difficult task, as is evident from 50-year long search for Fulde-Ferrell-Larkin-Ovchinnikov phase in Pauli-limited superconductors. Another question, what is the origin of many anomalies seen in multiple experimental probes in confined  $^3\text{He}$ ? Is it simply a technical difficulty that is related to the complexity and extreme environment of the system, or there exist new uncovered physics that is related to the unusual quasiparticle states? We are at a point where one might have high expectations that the next few years will bring us answers to many of these questions.

**Acknowledgements.** I would like to thank the Editors for inviting me to submit a manuscript for this theme issue.

**Funding statement.** The work on this review is supported by NSF through grant DMR-0954342.

**Conflict of interests.** I have no competing interests.

## References

1. Sigrist M, Ueda K. 1991 Phenomenological theory of unconventional superconductivity. *Reviews of Modern Physics* **63**, 239.
2. Andreev AF. 1964 Thermal conductivity of the intermediate state of superconductors. *Sov. Phys. JETP* **19**, 1228.
3. Herath J, Kurkijärvi J, Rainer D. 1990 Particle-hole coherence in superfluid  $^3\text{He}$  and in superconductors. *Czechoslovak Journal of Physics* **40**, 1156–1167.
4. Kieselmann G, Rainer D. 1983 Branch Conversion at Surfaces of Superfluid  $^3\text{He}$ . *Zeitschrift Fur Physik B-Condensed Matter* **52**, 267–275.
5. Zhang WY, Kurkijärvi J, Rainer D, Thuneberg EV. 1988 Andreev Scattering at a Rough-Surface of  $^3\text{He}$ -B. *Physical Review B* **37**, 3336–3343.
6. Jackiw R, Rebbi C. 1976 Solitons with Fermion Number 1/2. *Physical Review D* **13**, 3398–3409.
7. Matsumoto M, Shiba H. 1995 Coexistence of different symmetry order parameters near a surface in d-wave superconductors .2. *Journal Of The Physical Society Of Japan* **64**, 4867–4881.
8. Fogelström M, Rainer D, Sauls JA. 1997 Tunneling into current-carrying surface states of high- $T_c$  superconductors. *Physical Review Letters* **79**, 281–284.
9. Walter H, Prusseit W, Semerad R, Kinder H, Assmann W, Huber H, Burkhardt H, Rainer D, Sauls JA. 1998 Low-temperature anomaly in the penetration depth of  $\text{YBa}_2\text{Cu}_3\text{O}_7$  films: Evidence for Andreev bound states at surfaces. *Physical Review Letters* **80**, 3598–3601.
10. Higashitani S. 1997 Mechanism of Paramagnetic Meissner Effect in High-Temperature Superconductors. *Journal Of The Physical Society Of Japan* **66**, 2556–2559.
11. Kusama Y, Ohashi Y. 1999 Effect of the BCS supercurrent on the spontaneous surface flow in unconventional superconductivity with broken time-reversal-symmetry. *Journal Of The Physical Society Of Japan* **68**, 987–993.
12. Barash YS, Kalenkov MS, Kurkijärvi J. 2000 Low-temperature magnetic penetration depth in d-wave superconductors: Zero-energy bound state and impurity effects. *Physical Review B* **62**, 6665–6673.
13. Löfwander T, Shumeiko VS, Wendin G. 2000 Time-reversal symmetry breaking at Josephson tunnel junctions of purely d-wave superconductors. *Physical Review B* **62**, 14653–14656.
14. Bobkov AM, Zhu LY, Tsai SW, Nunner TS, Barash YS, Hirschfeld PJ. 2004 Electronic structure of d-wave superconducting quantum wires. *Physical Review B* **70**, 144502.
15. Ambegaokar V, Degennes PG, Rainer D. 1974 Landau-Ginsburg Equations for an Anisotropic Superfluid. *Physical Review A* **9**, 2676–2685.
16. Kjalldman LH, Kurkijärvi J, Rainer D. 1978 Suppression of P-Wave Superfluidity in Long, Narrow Pores. *Journal of Low Temperature Physics* **33**, 577–587.
17. Li YH, Ho TL. 1988 Superfluid  $^3\text{He}$  in very confined regular geometries. *Physical Review B* **38**, 2362.
18. Fetter AL, Ullah S. 1988 Superfluid density and critical current of  $^3\text{He}$  in confined geometries. *Journal of Low Temperature Physics* **70**, 515–535.



19. Wiman JJ, Sauls JA. 2013 Superfluid Phases of  $^3\text{He}$  in a Periodic Confined Geometry. *Journal of Low Temperature Physics* **175**, 17–30.
20. Aoyama K. 2014 Stripe order in superfluid  $^3\text{He}$  confined in narrow cylinders. *Physical Review B* **89**, 140502.
21. Ullah S. 1988 NMR in superfluid  $^3\text{He}$  in a confined geometry. *Physical Review B* **37**, 5010.
22. Eilenberger G. 1968 Transformation of Gorkov's equation for type II superconductors into transport-like equations - Springer. *Zeitschrift für Physik*.
23. Larkin AI, Ovchinnikov YN. 1969 Quasiclassical method in the theory of superconductivity. *Sov. Phys. JETP* **28**, 1200.
24. Serene JW, Rainer D. 1983 The quasiclassical approach to superfluid  $^3\text{He}$ . *Physics Reports* **101**, 221–311.
25. Kopnin NB. 1986 Dynamics of superfluid helium-3 in flow channels with restricted geometries. *Journal of Low Temperature Physics* **65**, 433–458.
26. Buchholtz LJ. 1993 Superfluid  $^3\text{He}$ -B in a realistic thin film. Gap and critical current. *Journal of Low Temperature Physics* **92**, 43–76.
27. Buchholtz L. 2000 Critical current states of superfluid  $^3\text{He}$  in a realistic channel. *Physica B-Condensed Matter* **284-288**, 273–274.
28. Yamamoto M, Higashitani S, Nagato Y. 2000 Superfluid density in  $^3\text{He}$  film. *Physica B-Condensed Matter* **284-288**, 271–272.
29. Hara J, Nagai K. 1988 Quasiclassical Green's function in slab geometry: Application to A-B transition of superfluid  $^3\text{He}$  in a slab. *Journal of Low Temperature Physics* **72**, 407–427.
30. Nagato Y, Nagai K. 2000 A–B transition of superfluid  $^3\text{He}$  in a slab with rough surfaces. *Physica B-Condensed Matter* **284-288**, 269–270.
31. Vorontsov AB, Sauls JA. 2003 Thermodynamic properties of thin films of superfluid  $^3\text{He}$ -A. *Physical Review B* **68**, 064508.
32. Tsutsumi Y, Ichioka M, Machida K. 2011 Majorana surface states of superfluid  $^3\text{He}$  A and B phases in a slab. *Physical Review B* **83**, 094510.
33. Wu H, Sauls JA. 2013 Majorana excitations, spin and mass currents on the surface of topological superfluid  $^3\text{He}$ -B. *Physical Review B* **88**, 184506.
34. Eschrig M. 2000 Distribution functions in nonequilibrium theory of superconductivity and Andreev spectroscopy in unconventional superconductors. *Physical Review B* **61**, 9061.
35. Buchholtz LJ, Rainer D. 1979 Quasiclassical Boundary-Conditions for Fermi Liquids at Surfaces. *Zeitschrift Für Physik B-Condensed Matter* **35**, 151–162.
36. Buchholtz LJ. 1986 Fermi Superfluids at a Rough-Surface. *Physical Review B* **33**, 1579–1584.
37. Buchholtz LJ. 1991 Superfluid  $^3\text{He}$ -B at a Rough-Surface - Density of States in the Randomly-Rippled-Wall Model. *Physical Review B* **44**, 4610–4617.
38. Zhang WY, Kurkijärvi J, Thuneberg EV. 1987 Order Parameter of Superfluid  $^3\text{He}$ -B Near Surfaces. *Physical Review B* **36**, 1987–1995.
39. Thuneberg EV, Fogelström M, Kurkijärvi J. 1992 Diffusely Scattering Surface in Superfluid  $^3\text{He}$ . *Physica B-Condensed Matter* **178**, 176–180.
40. Nagato Y, Higashitani S, Yamada K, Nagai K. 1996 Theory of rough surface effects on the anisotropic BCS states. *Journal of Low Temperature Physics* **103**, 1–22.
41. Nagato Y, Yamamoto M, Nagai K. 1998 Rough surface effects on the p-Wave Fermi superfluids. *Journal of Low Temperature Physics* **110**, 1135.



42. Eschrig M. 2009 Scattering problem in nonequilibrium quasiclassical theory of metals and superconductors: General boundary conditions and applications.  
*Physical Review B* **80**, 134511.
43. Hu CR. 1994 Midgap surface states as a novel signature for  $d_{x_a^2-x_b^2}$ -wave superconductivity.  
*Physical Review Letters* **72**, 1526.
44. Vorontsov A, Vavilov M, Chubukov A. 2010 Superconductivity and spin-density waves in multiband metals.  
*Physical Review B* **81**, 174538.
45. Sauls JA. 2011 Surface states, edge currents, and the angular momentum of chiral p-wave superfluids.  
*Physical Review B* **84**, 214509.
46. Tsutsumi Y, Machida K. 2012 Edge mass current and the role of Majorana fermions in A-phase superfluid  $^3\text{He}$ .  
*Physical Review B* **85**, 100506.
47. Kosztin I, Leggett AJ. 1997 Nonlocal effects on the magnetic penetration depth in d-wave superconductors.  
*Physical Review Letters* **79**, 135–138.
48. Nagato Y, Nagai K. 1995 Surface and size effect of a  $d_{xy}$ -state superconductor.  
*Physical Review B* **51**, 16254.
49. Vorontsov AB. 2009 Broken Translational and Time-Reversal Symmetry in Unconventional Superconducting Films.  
*Physical Review Letters* **102**, 177001.
50. Hara J, Nagai K. 1986 A Polar State in a Slab as a Soluble Model of p-Wave Fermi Superfluid in Finite Geometry.  
*Progress of Theoretical Physics* **76**, 1237–1249.
51. Saint-James D, Sarma G, Thomas E. 1968 *Type-II Superconductivity*. Pergamon Press.
52. Håkansson M, Löfwander T, Fogelström M. 2014 Spontaneously broken time-reversal symmetry in high-temperature superconductors.  
*arXiv.org:1411.0886v1*.
53. Vorontsov AB, Sauls JA. 2007 Crystalline Order in Superfluid  $^3\text{He}$  Films.  
*Physical Review Letters* **98**, 045301.
54. Salomaa M, Volovik G. 1988 Cosmiclike domain walls in superfluid  $^3\text{He}$  B: Instantons and diabolical points in  $(\mathbf{k}, \mathbf{r})$  space.  
*Physical Review B* **37**, 9298–9311.
55. Silveri M, Turunen T, Thuneberg E. 2014 Hard domain walls in superfluid  $^3\text{He}$ -B.  
*Physical Review B* **90**, 184513.
56. Vorontsov A, Sauls JA. 2005 Domain Walls in Superfluid  $^3\text{He}$ -B.  
*Journal of Low Temperature Physics* **138**, 283–288.
57. Miyawaki N, Higashitani S. 2015 Fermi surface effect on spontaneous breaking of time-reversal symmetry in unconventional superconducting films.  
*Physical Review B* **91**, 094511.
58. Hachiya M, Aoyama K, Ikeda R. 2013 Field-induced reentrant superconductivity in thin films of nodal superconductors.  
*Physical Review B* **88**, 064519.
59. Higashitani S, Miyawaki N. 2015 Phase Transition to a Time-Reversal Symmetry-Breaking State in d-Wave Superconducting Films with Rough Surfaces.  
*Journal Of The Physical Society Of Japan* **84**, 033708.
60. Löfwander T, Shumeiko VS, Wendin G. 2001 Andreev bound states in high-T-c superconducting junctions.  
*Superconductor Science and Technology* **14**, R53–R77.
61. Deutscher G. 2005 Andreev–Saint-James reflections: A probe of cuprate superconductors.  
*Reviews of Modern Physics* **77**, 109.
62. Carmi R, Polturak E, Koren G, Auerbach A. 2000 Spontaneous macroscopic magnetization at the superconducting transition temperature of  $\text{YBa}_2\text{Cu}_3\text{O}_{7-\delta}$ .  
*Nature* **404**, 853–855.
63. Elhalel G, Beck R, Leibovitch G, Deutscher G. 2007 Transition from a Mixed to a Pure d-Wave Symmetry in Superconducting Optimally Doped  $\text{YBa}_2\text{Cu}_3\text{O}_{7x}$  Thin Films Under Applied Fields.

- Physical Review Letters* **98**, 137002.
64. Saadaoui H, Morris GD, Salman Z, Song Q, Chow KH. 2011 Search for broken time-reversal symmetry near the surface of superconducting  $\text{YBa}_2\text{Cu}_3\text{O}_{7-\delta}$  films using  $\beta$ -detected nuclear magnetic resonance.  
*Physical Review B* **83**, 054504.
  65. Gustafsson D, Golubev D, Fogelström M, Claeson T, Kubatkin S, Bauch T, Lombardi F. 2012 Fully gapped superconductivity in a nanometre-size  $\text{YBa}_2\text{Cu}_3\text{O}_{7-\delta}$  island enhanced by a magnetic field.  
*Nature Nanotechnology* **8**, 25–30.
  66. Aoki Y, Wada Y, Saitoh M, Nomura R, Okuda Y. 2005 Observation of Surface Andreev Bound States of Superfluid  $^3\text{He}$  by Transverse Acoustic Impedance Measurements.  
*Physical Review Letters* **95**, 075301.
  67. Murakawa S, Tamura Y, Wada Y, Wasai M, Saitoh M. 2009 New Anomaly in the Transverse Acoustic Impedance of Superfluid  $^3\text{He}$ -B with a Wall Coated by Several Layers of  $^4\text{He}$ .  
*Physical Review Letters* **103**, 155301.
  68. Okuda Y, Nomura R. 2012 Surface Andreev bound states of superfluid  $^3\text{He}$  and Majorana fermions.  
*Journal Of Physics-Condensed Matter* **24**, 343201.
  69. Choi H, Davis JP, Pollanen J, Halperin WP. 2006 Surface specific heat of  $^3\text{He}$  and Andreev bound states.  
*Physical Review Letters* **96**, 125301.
  70. Sachrajda A, Harrislowe RF, Harrison JP, Turkington RR, Daunt JG. 1985  $^3\text{He}$  Film Flow - Two-Dimensional Superfluidity.  
*Physical Review Letters* **55**, 1602–1605.
  71. Davis J, Amar A, Pekola J, Packard R. 1988 Superfluidity of  $^3\text{He}$  Films.  
*Physical Review Letters* **60**, 302–304.
  72. Daunt JG, Harrislowe RF, Harrison JP, Sachrajda A, Steel S, Turkington RR, Zawadzki P. 1988 Critical-Temperature and Critical Current of Thin-Film Superfluid  $^3\text{He}$ .  
*Journal of Low Temperature Physics* **70**, 547–568.
  73. Steel SC, Harrison JP, Zawadzki P, Sachrajda A. 1994  $^3\text{He}$  film flow on a round rim beaker.  
*Journal of Low Temperature Physics* **95**, 759.
  74. Xu J, Crooker B. 1990 Very thin films of  $^3\text{He}$ : A new phase.  
*Physical Review Letters* **65**, 3005–3008.
  75. Schechter AMR, Simmonds R, Packard R, Davis J. 1998 Observation of ‘thirdsound’ in superfluid  $^3\text{He}$ .  
*Nature* **396**, 554.
  76. Saitoh M, Ikegami H, Mukuda H, Kono K. 2003 Study of dynamical properties of superfluid  $^3\text{He}$  film flow by inter-digitated capacitors.  
*Physica B-Condensed Matter* **329**, 131–132.
  77. Saitoh M, Ikegami H, Mukuda H, Kono K. 2004 Measurement of Superfluid  $^3\text{He}$  Film Flow by Inter-digitated Capacitors.  
*Journal of Low Temperature Physics* **134**, 357.
  78. Saitoh M, Kono K. 2007 Thickness Dependence of Critical Current of Superfluid  $^3\text{He}$  Film.  
*Journal of Low Temperature Physics* **148**, 483–487.
  79. Freeman M, Germain R, Thuneberg E, Richardson R. 1988 Size effects in thin films of superfluid  $^3\text{He}$ .  
*Physical Review Letters* **60**, 596–599.
  80. Kawae T, Kubota M, Ishimoto Y, Miyawaki S, Ishikawa O, Hata T, Kodama T. 1998 A-B transition of superfluid  $^3\text{He}$  with a film geometry.  
*Journal of Low Temperature Physics* **111**, 917–935.
  81. Miyawaki S, Kawasaki K, Inaba H, Matsubara A, Ishikawa O, Hata T, Kodama T. 2000 Pressure dependence of the  $A - B$  phase transition temperature in superfluid  $^3\text{He}$  in  $1.1\text{-}\mu\text{m}$  slab geometry.  
*Physical Review B* **62**, 5855.
  82. Kawasaki K, Yoshida T, Tarui M, Nakagawa H, Yano H, Ishikawa O, Hata T. 2004 Phase-Transition Phenomena of  $0.8\text{ }\mu\text{m}$  Superfluid  $^3\text{He}$  Slab.  
*Physical Review Letters* **93**, 105301.
  83. Levitin LV, Bennett RG, Casey A, Cowan B, Saunders J, Drung D, Schurig T, Parpia JM. 2013 Phase Diagram of the Topological Superfluid  $^3\text{He}$  Confined in a Nanoscale Slab Geometry.

- Science* **340**, 841–844.
84. Levitin LV, Bennett RG, Casey A, Cowan B, Saunders J, Drung D, Schurig T, Parpia JM, Ilic B, Zhelev N. 2014 Study of Superfluid  $^3\text{He}$  Under Nanoscale Confinement.  
*Journal of Low Temperature Physics* **175**, 667–680.
  85. Gonzalez M, Bhupathi P, Moon BH, Zheng P, Ling G, Garcell E, Chan HB, Lee Y. 2011 Characterization of MEMS Devices for the Study of Superfluid Helium Films.  
*Journal of Low Temperature Physics* **162**, 661–668.
  86. Gonzalez M, Zheng P, Garcell E, Lee Y, Chan HB. 2013 Comb-drive micro-electro-mechanical systems oscillators for low temperature experiments.  
*Review of Scientific Instruments* **84**, 025003.
  87. Gonzalez M, Zheng P, Moon BH, Garcell E, Lee Y, Chan HB. 2013 Unusual Behavior of a MEMS Resonator in Superfluid He-4.  
*Journal of Low Temperature Physics* **171**, 200–206.
  88. Rojas X, Davis JP. 2015 Superfluid nanomechanical resonator for quantum nanofluidics.  
*Physical Review B* **91**.
  89. Fujita T, Nakahara M, Ohmi T, Tsuneto T. 1980 A-B Transition in Superfluid Helium-3 Film.  
*Progress of Theoretical Physics* **64**, 396–405.